Optimisation of a Photovoltaic-Thermal (PV-T) panel for Desalination

S. A. Mhatre

Technische Universiteit Delft

TU Delft Delft University of Technology

Optimisation of a Photovoltaic-Thermal (PV-T) Panel for Desalination

by

Supriya A. Mhatre

to obtain the degree of Master of Science
at the Delft University of Technology,
to be defended publicly on Wednesday August 26, 2020 at 10:00 AM.

Student number:	4867831	
Project duration:	November, 2019 – August, 2020	
Thesis committee:	Dr. ir. Olindo Isabella,	TU Delft, Supervisor
	Dr. ir. Hesan Ziar,	TU Delft, Daily supervisor
	Dr. ir. Jiajun Cen,	Desolenator, Company supervisor
	Dr. ir. Zian Qin,	TU Delft, External committee member

This thesis is confidential and cannot be made public until August 26, 2022.

TU Delft

Abstract

Water stress levels are rising due to industrialization and the increase in population. With the freshwater supplies depleting at a rate faster than the refreshment rate, there is a need to look into unconventional and sustainable sources of water. Desalination technology is a reliable solution for the future water requirement; however, it is an energy-intensive process. Desalination is mostly powered by fossil fuels and there is a need to move away from these. For this reason, a Photovoltaic Thermal (PV-T) powered desalination plant which uses the Multi-effect Distillation (MED) coupled with Mechanical Vapour Compression (MVC) technology, is investigated. A novel design of the PV-T module is used wherein a water reservoir is attached directly to the back of a PV module.

The PV-T module produces electrical and thermal energy simultaneously, which are the required inputs to a MED-MVC desalination system. To have the desalination system working efficiently, it is important to predict the output from the module with respect to its design and the location weather parameters. To predict the output water temperature with varying weather conditions, a PV-T model was built using COMSOL Multiphysics. The model was validated using experimental data from the location of Dubai. It is found that the water outlet temperature and the total efficiency of the module vary with its inclination angle and flow rate of water through it. With a sensitivity analysis for the outlet water temperature and the total efficiency with respect to tilt angle and flow rate, optimum values for these parameters are obtained for summer and winter days. A maximum water outlet temperature of 91^o C in summer and 58^o C in winter is predicted from the model, for the Dubai location, for these optimum values. Using experimental and simulated results, output parameters such as water outlet temperature at a given flow rate is predicted using dimensionless numbers which characterises the PV-T design and the surrounding environment that the system is placed in.

The hot water from the PV-T array which consists of 400 PV-T panels is used to produce steam using flash evaporation, for thermal input to the MED vessel. Sensitivity analysis for the temperature and quantity of the hot water produced from the array, showed that a maximum amount of steam of 1782 kg can be produced on a summer day with a water outlet temperature of 85^o C. Due to lower water outlet temperature in winter, heating elements should be used to raise the water temperature to 85^o C. The maximum amount of steam produced, as a result of 85^o C water temperature, will lead to 6058 kg of distilled water per day when used as input to the MED with 4 effects. According to water requirement, additional steam can be produced by the MVC.

Acknowledgements

I would like to express my gratitude to everyone for their kind help and support during my thesis journey.

I would like to thank Dr Hesan Ziar, my daily supervisor, for his insights and guidance, for being so patient, and for motivating me throughout this thesis work. I would like to thank my main supervisor, Dr Olindo Isabella, for his valuable suggestions and for always giving time out of his schedule whenever I needed. I am thankful to my company supervisor, Dr Jiajun Cen for his ideas and recommendations, and for being available whenever I needed help. I would also like to thank Dr Zian Qin for being part of my thesis committee.

I would like to express my appreciation to the PVMD department and the Desolenator team for their valuable feedback and help at various times. I would also like to thank Catriona Mcgill and William Janssen for being so supportive in my work and for all their suggestions. Special thanks to Rob, Sam and Amit for providing me with all the valuable information on the processes. Thank you to Lyndon for being so kind and sharing the knowledge on COMSOL with me.

Thank you to all my friends for their support and helping me stay sane. Special thanks to Barad for always encouraging and supporting me. Finally, thank you to my family for their love and support, and without whom this would not have been possible.

Contents

List of Tables

List of Figures

List of Abbreviations

AM	Air Mass
ARC	Anti-reflective coating
c-Si	Crystalline silicon
DHI	Diffuse horizontal irradiance
DNI	Direct normal irradiance
ED	Electrodialysis
EPDM	Ethylene Propylene Diene Monomer
EVA	Ethyl Vinyl Acetate
FEM	Finite Element Method
GHI	Global horizontal irradiance
GOR	Gained Output Ratio
IDA	International Desalination Association
MENA	The Middle East and North Africa
MED	Multi-Effect Distillation
MSF	Multistage Flash Distillation
MVC	Mechanical Vapour Compression
PIR	Polyisocyanurate Foam
PPM	Parts per Million
PR	Performance Ratio
PV	Photovoltaic
PVMD	Photovoltaic Materials and Devices
PVT	Photovoltaic Thermal
STC	Standard Test Conditions
TVC	Thermovapour Compressor
VC	Vapour compression

List of Symbols

ΔT	Temperature difference between the fluid inlet and outlet
$\dot{m}$	mass flow rate (kg/s)
ϵ	Emissivity
η_{PV}	Electrical efficiency
η_{th}	Thermal efficiency
η_{total}	Total efficiency
μ	Dynamic viscosity (Ns/m^2)
ρ	Density (kg/m^3)
σ	Stefan Boltzmann constant
a_{S}	Surface area (m^2)
A	Absorption factor
C_p	Specific heat capacity (J/kgK)
E	Emitted power
Gr	Grashof number
h	Heat transfer coefficient (W/m^{2}K)
H_v	Vaporisation enthalpy at saturation temperature (J/kg)
I	Irradiance (W/m^2)
k	Thermal conductivity (W/mK)
l	Hydraulic diameter (m)
m_s	Mass of steam (kg)
m_w	Mass of liquid water (kg)
Nu	Nusselt number (ql/kΔT)
P	Power generated (W)
Pr	Prandtl number ($C_p\mu$/k)
q	Heat flux (W/m^2)
Re	Reynolds number (ρvl/μ)
T_in	Inlet temperature
T_out	Outlet temperature
T_f	Fluid temperature
T_{if}	Initial temperature of water to flash vessel (K)
T_{st}	Saturation temperature of water (K)
T_s	Surface temperature
v	Inlet velocity of fluid (m/s)

1 Introduction

1.1. Background

Water stress levels are rising due to the growing demand for water, with an increase of 1% per year, and due to climate change effects. 71% of the planet is covered in water, yet, 25% of the population has restricted access to clean and safe water [50]. Additional stresses would be created in regions with currently abundant water resources, and the situations in water-stressed regions are likely to be worsened due to changes in the precipitation patterns as a result of the changing climate.

The ratio of water withdrawal to the total available supply, known as the baseline water stress, for the year 2019, is seen in Figure 1.1. 50% of the global population is expected to be living in regions with high water stress by the year 2025 [53]. Globally, a 40% deficit in the global water supply is predicted by 2030 [1]. The availability of water impacts not only the basic human rights for water and sanitation but also proves to be a threat to several socio-economic factors such as agriculture, energy production and settlements, as seen in Figure 1.2. [50].

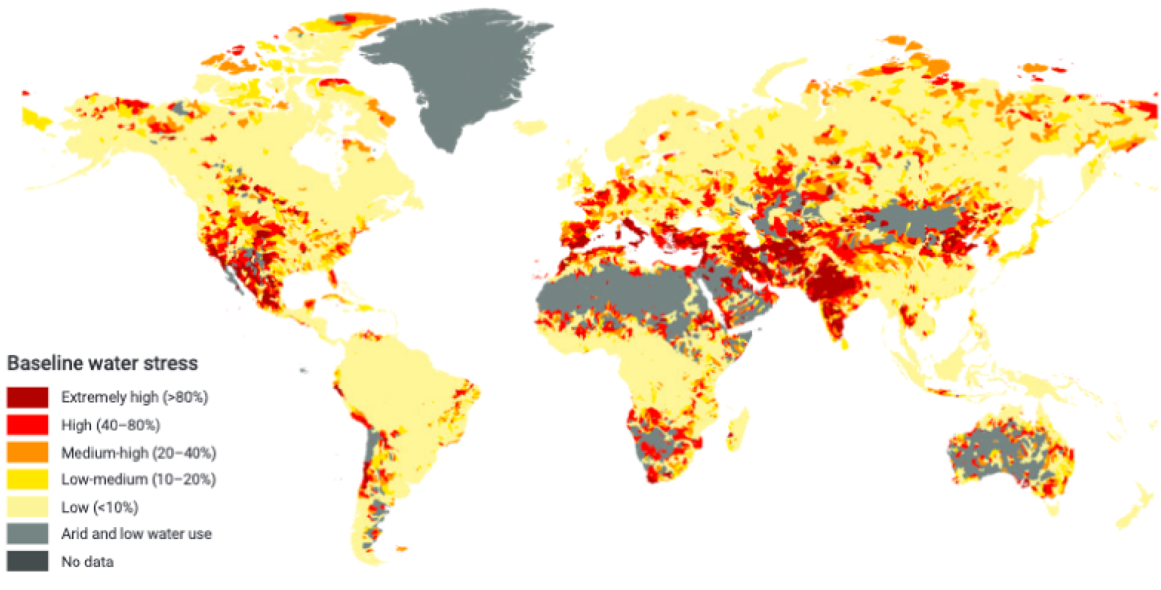

Figure 1.1: Global annual baseline water stress in 2019. [50]

The warm and arid MENA regions (the Middle East and North Africa) and parts of South Asia face severe water shortages due to infrequent rainfall and the increasing groundwater salinity [35]. The freshwater resources

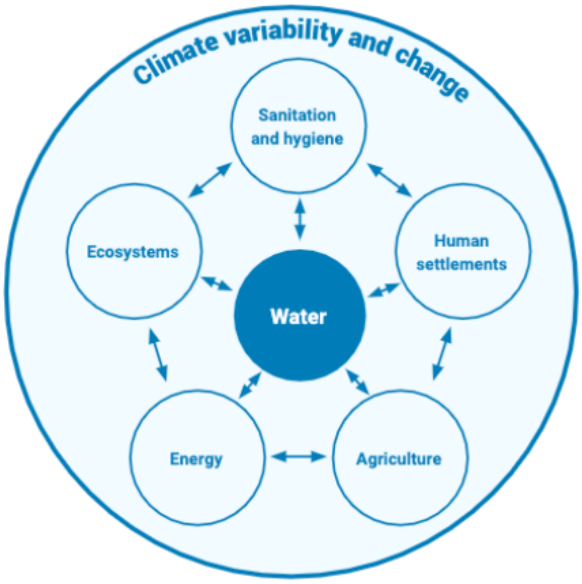

Figure 1.2: The socio-economic factors dependent on water. [50]

available in these regions are depleting due to increase in population, industrialization and agricultural activities. Therefore the costs of water in these regions are high compared to costs of water with conventional sources like freshwater from rivers, lakes and ponds. The locations which are remote and rural with a low population density, make the transportation of water difficult [35]. The transportation of water to these regions have large costs which increase depending on the distances to be covered. It also includes the cost of a storage system that is required for transport. Pipelines restrict the possibility of increasing the flow rate if additional capacity is required in future [4]. This calls for urgent action to look into unconventional and sustainable water resources for the future.

A number of countries facing water shortages depend on desalinated water. Thermal desalination processes follow the principle of the natural hydrological cycle along with energy sources for evaporation and condensation [35].

1.2. Need for Desalination

Desalination is a reliable solution to meet our future water demands and the process has been commercially practised over decades [51]. Desalination technology extracts salts from saline water and gives clean water as the output. Using desalination for the water requirement also provides an option for increasing the capacity if required, unlike water transport to remote locations through pipes. When plants are located near the coast, it eases its operation as less energy is required for pumping water [4]. Additionally, it solves the issue of brine disposal by discharging it into the sea without damaging the soil or groundwater sources.

Desalination technology is extremely expensive in terms of energy cost and is environmentally pollutive. It requires high energy consumption for the removal of salts and thus leads to higher greenhouse gas emissions as it is mostly fossil fuel-powered [28]. Currently, desalination accounts for 0.4% of global electricity consumption and 200 million tons of carbon emissions per year [47]. To produce 1 m^3 of freshwater per day, by desalination, 10 tons of oil is required per year [26]. This is equivalent to providing electricity to 38 Dutch households for a year. The energy costs for desalination accounts for 50-70% of the costs, therefore, it is economical only when the energy costs are low [32, 51]. Only a few of the dry regions, who have abundant oil resources can actually afford these huge costs. Other economically poor regions neither have abundant oil reserves nor have the money to import these huge amounts of oil [35]. Often water-short regions are rich in renewable energy sources. These sources can be coupled with desalination plants for its energy requirements to setup low scale desalination plants in remote locations [35].

Solar energy is an abundant renewable energy source in dry regions and solar desalination is a much cleaner and economical solution. The first solar distillation plant was developed in Chile, in the year 1872. It was a simple wooden structure covered with a glass cover and had a capacity of 22.5 m^3/day [32]. According to the International Desalination Association (IDA) in 100 m^3/day plants throughout the world, a total of 16 million m^3/day capacity was produced by the 1990s, 67% of which was used for drinking and the remaining for agricultural and industrial use [32].

The commonly used processes for desalination are the Multi-Effect Distillation (MED), Multistage flash Distillation (MSF), Reverse Osmosis (RO), Electrodialysis (ED), and Vapour Compression (VC); of which the MED and MSF are leading technologies for thermal desalination [30, 51]. These energy-intensive processes can be made sustainable by using renewable energy sources for their energy requirement [51]. The heat generated from electrical production can be used as low-cost heat in thermal desalination plants. These cogeneration plants save up to 26% energy compared to plants that do not produce its own electricity and also reduces the CO_2 emissions per m^3 of water produced [32].

1.2.1. Solar desalination

Solar-MED is the renewable desalination combination investigated in this report. The solar energy can be used to pre-heat water and generate the steam required by the desalination plant. Solar energy as a renewable source with energy back up is one of the most cost-competitive methods of desalination [51]. For regions with high irradiance and temperature levels, Photovoltaic Thermal (PV-T) collectors can be used to capture solar energy. A typical crystalline silicon module converts around 20% of the incident irradiance into electricity and the rest is lost in the form of heat. In a PV-T module, this heat is captured in the form of heating water. Thus, this electrical and thermal energy produced can be used in the desalination process [6].

1.3. Photovoltaic-Thermal (PV-T) Module

A Photovoltaic Thermal (PV-T) module produces electricity and heat simultaneously. PV-T modules have been researched since the 1970s with its initial aim being to improve the electrical efficiency of the PV cells [2]. A PV module loses efficiency when there is an increase in its temperature. PV modules are rated at standard test conditions (STC) of irradiance 1 kW/m^2 and temperature of 25^o C. Above this temperature the rated power output decreases, thus decreasing the efficiency of the module. This reduction in output is given by the temperature coefficient of the particular solar cell technology, the value of which is given by the PV manufacturer on its datasheet [11, 46]. The average value for the power temperature coefficient for a monocrystalline silicon module was found to be -0.446 %/^{o} C [11]. In a PV-T panel, a heat extracting fluid flows in metal tubes behind a PV panel thus extracting heat from the panels and cooling the cells whilst maintaining electrical efficiency.

The PV-T panel designed by Desolenator is a novel design wherein the water reservoir is attached directly beneath the PV panels to allow for most efficient heat transfer from the panel to the cooling liquid [6].

1.4. Project Outline

Desolenator is developing a solar desalination plant for the Dubai Electricity and Water Authority (DEWA). This community unit is a stand-alone system designed to operate continuously using solar energy as the sole energy source. The system includes a solar PV-T powered Multi-Effect Distillation (MED) with Mechanical Vapour Compression (MVC), which converts seawater into distilled water, producing about 10,000 litres every day. The PV-T array will produce both electrical and thermal energy. The electrical energy will be used for the electrical requirements of pumps, heating elements, and other auxiliary systems. The thermal energy (hot water) produced by the panel will be used to generate steam at sub-atmospheric pressure which will be used to drive the MED system to produce distilled water from seawater. The excess electrical energy generated by the PV-T panels will be stored in batteries, and excess hot water is stored in insulated hot water tanks. During the night (no sunlight hours) the MED will operate on a minimal partial load of about 45% of the daytime load using this stored energy. **The aim is to develop an economical and efficient desalination plant.** A schematic of the plant can be seen in Figure 1.3.

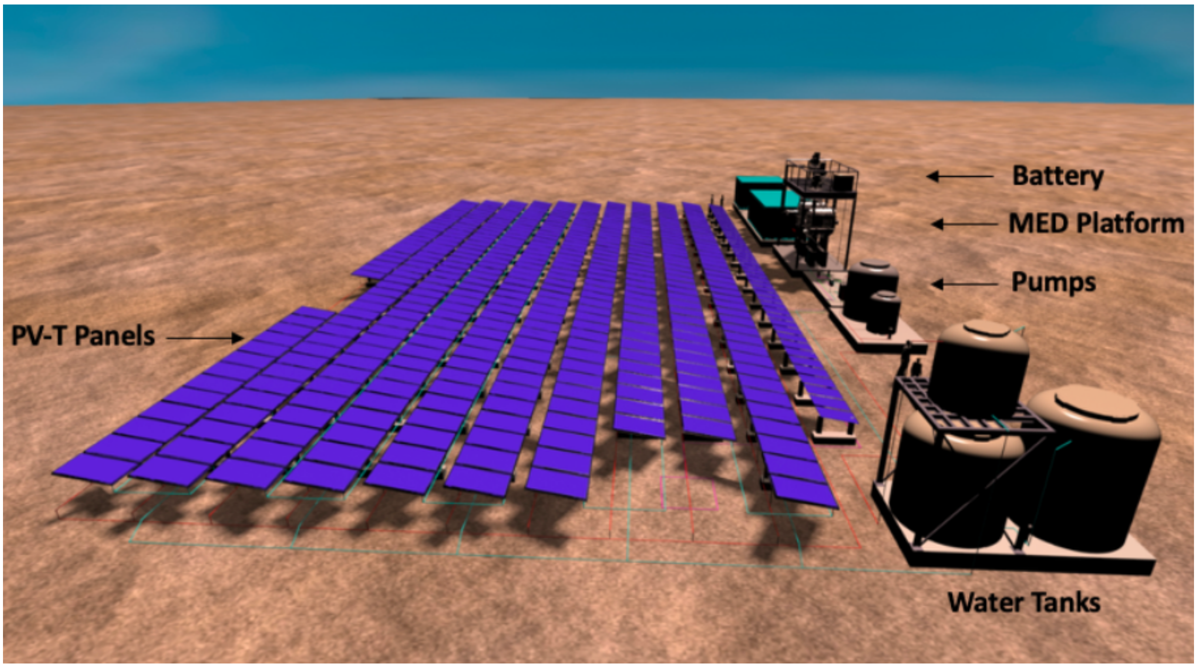

Figure 1.3: Schematic of the plant.

1.5. Research Objectives

Available tools from literature for the prediction of electrical plus thermal output of a PV-T module are limited to the type of design or location, with no simplified models considering the heat losses involved. To design an efficient solar desalination system, it is desirable to know the PV-T module output estimates depending on the particular location's weather parameters. **This research focusses on developing and validating a tool for predicting the total output of a PV-T system (electrical+ thermal) for the desired location.** Thus, a Finite element method (FEM model) of the PV-T panel will be developed in COMSOL Multiphysics and validated using experimental results. Based on results from the model, a relationship between the output, design and location parameters is derived. Output parameters such as water outlet temperature at a given flow rate is predicted using dimensionless numbers which characterises the PV-T design and the surrounding environment the system is placed in.

The incidence of solar irradiance on a PV module affects the module performance. As the incidence on the module increases, the power output and efficiency increase [22]. Therefore, it is necessary to install the modules at an optimum tilt angle at which the incident irradiance on the module is maximum. The position of the sun depends on the location of installation and changes with the time of the day and year [46]. It is practically not possible to vary the tilt angle every month during a year. Therefore, a yearly optimum tilt to capture maximum solar irradiation throughout the year is usually selected [22]. With the technological nature of Desolenator's PV-T design, it may not be practical to install them at this optimum angle owing to the flowing water in them. Therefore, a study on the effect of varying tilt angles on the output of the module will be done for the location of Dubai, UAE, which is the site of the plant.

It has been found that varying the flow rate through the PV-T system has an influence on its performance [14, 25, 34, 48]. Flowing water extracts heat from the backside of the panel, thereby cooling it relatively. This amount of heat extracted depends on the volume and speed of fluid passing through it. Therefore, a study on the effect of varying flow rates on the maximum outlet water temperature and efficiency of the module will be undertaken so that the most optimum flow rate can be selected for the plant location.

A similar sensitivity study will then be done with respect to tilt angle and flow rate for a different location, (West Bengal, India) to compare the effect on the module output for the two locations.

The output of the PV-T module is used as input to the MED-MVC desalination system. The quantity and temperature of hot water produced affect the production of distilled water from the system. Therefore, this effect of output on the MED-MVC desalination system will be analysed.

1.6. Outline of Thesis

This thesis is divided into seven chapters. In the first chapter, the background and need for desalination were presented. An overview of the PV-T and the plant design are given, and finally, the focus of this research is presented.

In the second chapter, the previous work into PV-T technology and the commonly used types of desalination processes will be discussed with the choice of the PV-T + MED-MVC combination. A detailed description of the PV-T panel design and the plant dynamics will be given in chapter three.

In chapter four, the methods used for modelling are described-the Buckingham's pi theorem, heat source definition within the module, electrical yield and finally, the developed COMSOL model is discussed. The heat transfer physics of conduction, convection and radiation on the panel, the model geometry definition, material and physics selection, and, model inputs are explained.

Chapter five shows the modelling results. First, the model validation with the experimental test data is discussed. Next, results from a sensitivity analysis for the location of Dubai and West Bengal for the summer and winter months are presented. And finally, the relationship derived using Buckingham's pi theorem is discussed. In chapter six, a sensitivity analysis w.r.t module output for steam generation and module to plant level scaling is undertaken, and finally, its effect on the MED output is analysed.

Finally, in chapter seven the conclusions and recommendations from the results are given and future work is discussed.

2
Literature Review

The PV-T technology concepts and previous work will be discussed in this chapter. The different configurations studied from literature and their performance results will be presented. Next, an overview of the most commonly used desalination technologies will be given with their advantages and disadvantages.

2.1. Photovoltaic-Thermal Technology

A PV-T module converts solar energy incident on its surface to electrical and thermal energy simultaneously, as seen in Figure 2.1. It consists of a PV module behind which a heat extracting fluid extracts heat from the module thus maintaining its operating temperature and thereby, the electrical efficiency. The extracted thermal energy (heat) can be used for applications like heating water for domestic use, space heating, agricultural use, and desalination [6, 7].

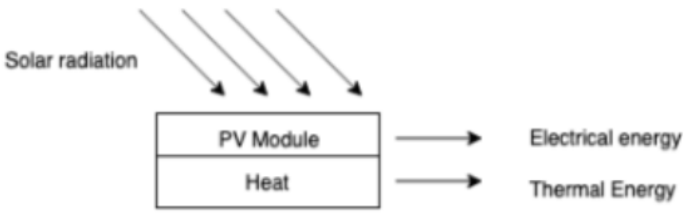

Figure 2.1: Concept of PV-T module.

The yield of the PV-T system is defined as the total useful energy obtained. The thermal and electrical efficiency is the total useful energy obtained upon the incident energy. Thermal efficiency is calculated by,

$$\eta_{th} = \dot{m}C_p\,(T\_out - T\_in)\,/\,Ia_S \tag{2.1}$$

Where $\dot{m}$ is the mass flow rate of fluid (kg/s), C_p is the specific heat capacity of the fluid (J/kgK), T_out and T_in is the outlet and inlet temperature respectively (K), I is the Irradiance on the panel (W/m^2) and a_S is the surface area of the PV-T panel. (m^2)

The electrical efficiency is calculated by,

$$\eta_{PV} = P\,/\,Ia_S \tag{2.2}$$

where P is the power generated by the PV module (W).

The electrical efficiency of a PV-T module is lower than that of a conventional PV module, and the thermal efficiency is lower than that of a solar thermal collector. The thermal and electrical efficiency was found to be 33% and 6.7% respectively for the PV-T combination for hot water production compared to 54% thermal for a conventional solar thermal collector and 7.2% electrical for conventional PV, in a study by Zondag [56]. However, the area used by a PV-T module harvests more energy compared to the same area with one PV module and one conventional solar collector. This also reduces the cost of installation and is architecturally pleasing [56]. For the PV-T design investigated by Cen et al., an electrical efficiency of 13% and thermal efficiency of 53% was obtained [6].

PV-T modules are either Flat plate PV-T or Concentrating PV-T. Concentrating PV-Ts use concentrators to focus the irradiation on the PV module to increase its incidence and thereby the yield. This report will discuss only the flat plate PV-T modules. Flat plate PV-T modules are further classified according to the heat extraction medium and fluid type-water and air; which are further classified based on the flow patterns.

According to a study by Prakash, the air type collectors are less efficient than water type collectors due to the lower heat transfer coefficient of air. The thermal efficiency for the water type design is observed to be between 50 to 70% compared to 17-51% for the same design with air as the fluid [34]. The water type PV-T modules are classified into; Sheet and tube type; Channel type; Free flow type and Two absorber type.

2.1.1. Sheet and tube type

The sheet and tube design is made by combining a conventional solar collector and a PV module as seen in Figure 2.2. A glass cover is fitted on top of the PV panel in order to reduce heat loss from the surface to ambient. However, studies show that the glass cover reduces the irradiance transmittance to the PV cells due to reflections at the glass and thus reduce the electrical efficiency. The reduction in electrical efficiency was found to be 0.8% with one glass cover and 1.6% with a double glass cover [55]. The optical losses in the performance ratio, which is the ratio of the obtained electrical efficiency with the efficiency of the module at STC, due to glass cover are found to be 8% for a cover without ARC and around 3.5% for glass cover with ARC on both sides [40]. The design without glass cover, on the other hand, produces higher electrical energy as there is no reflection of the incident irradiation and the PV cells have a cooling effect due to convection instigated by wind. However, it has a lower thermal efficiency due to heat loss from the surface compared to the thermal efficiency of a panel with a glass cover [38, 55]. The losses in the electrical efficiency with a glass cover are considered to be equal in magnitude to the thermal efficiency losses with no glass cover [55].

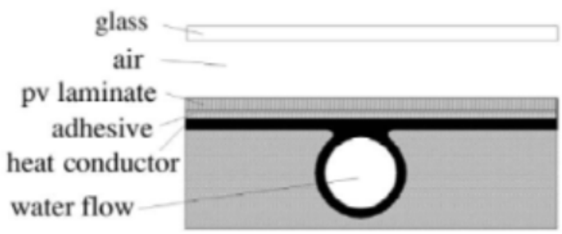

Figure 2.2: Sheet and tube type PV-T. [55]

2.1.2. Channel type

The channel type design has a water channel placed above the PV panel as seen in Figure 2.3. The glass sheet must be robust so as to not break due to the pressure of water below it. Also, the absorption spectrum of the fluid should differ from that of the silicon cells, else there is a loss in the irradiance reaching the PV layer, resulting in a lower electrical yield. There is an overlap between the absorption spectrum of water and silicon which resulted in a 4% decrease in its electrical efficiency, in a study by Zondag [55].

A modification to this type is the water channel below the PV layer. In this case, the PV module should be robust and leak proof so that water does not come in contact with the cell connections.

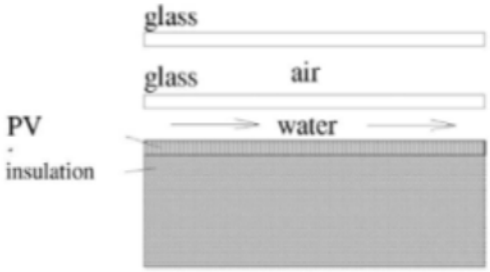

Figure 2.3: Channel type PV-T. [55]

2.1.3. Free flow type

The free flow design allows water to flow over the PV layer without any restriction as seen in Figure 2.4. This eliminates the requirement of a second glass cover as in case of the channel type, and thus reduces costs. As there is no double glass cover, it also reduces reflection losses. However, the issue of overlap in the absorption spectrum of water and silicon still needs to be addressed. Also, at higher temperatures, the water evaporates and condenses on the top glass causing additional reflection losses.

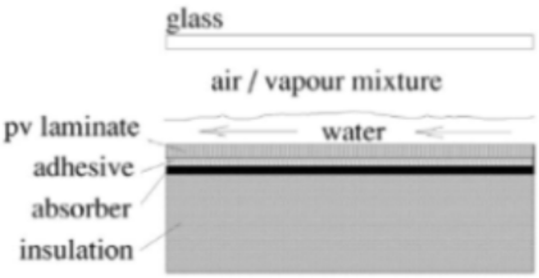

Figure 2.4: Free flow type PV-T. [55]

2.1.4. Two absorber type

This type consists of two absorbers and channels. The water flows in from the upper channel and goes out through the lower channel as in Figure 2.5. The glass must be strong enough to withstand water pressures which increase the costs of the design. Also, a second absorber increases costs.

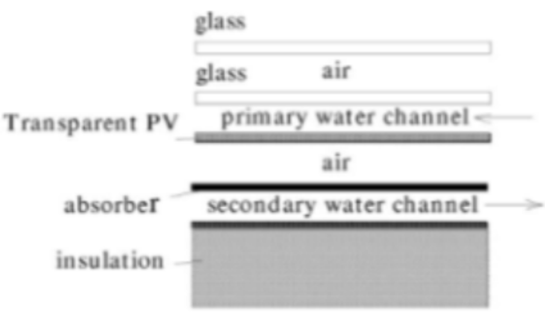

Figure 2.5: Two absorber type PV-T. [55]

Zondag et al., modelled and analysed the above types for their performance and efficiency [55]. The thermal efficiency of the channel, free flow and two absorber type was found to be higher than that of the sheet and

Table 2.1: Thermal and Electrical efficiency comparison of PV-T configurations. [55]

Type	Thermal efficiency(%)	Electrical efficiency (%)
Sheet and tube	58	8.9
Channel above PV	65	8.4
Channel below PV	60	9.0
Free flow	64	8.6
Two absorber	66	8.5

tube type as seen from Table 2.1. Taking into account the additional material costs for the channel and two absorber type, the free flow type is a promising option.

The mass flow rate of water through the module has shown to have an influence on the system performance [7, 14]. The heat transfer coefficient increases with an increase in the inlet velocity of water. Thus, the heat transfer to water increases, thereby cooling the cells whilst gaining thermal energy [7].

Kalogirou modelled and simulated a sheet and tube type PV-T system using TRYNSYS software, to study the effect of flow rate of water on the system output, during summer and winter, for the location of Nicosia, Cyprus [25]. The total efficiency of the system increased to up to 32% with an increase in the flow rate until 25kg/h and then decreased, as seen in Figure 2.6. This low flow rate indicates that it is possible to use the system without pumps, in thermosiphon mode which would reduce the initial as well as operating costs. Thermosiphon is a passive heat exchange method wherein the cooler liquid settles at the bottom due to higher density and the warmer liquid floats on top of the cooler liquid. Thus warmer liquid flows out of the system as it is replaced with a cooler fluid. The outlet should, therefore, be at a height above inlet from where the colder liquid flows in. The electrical efficiency of this system increased to 8% until a flow rate of 25 kg/h and was constant for a further increase in flow rate. It was also found that the electrical efficiency is lower in summer compared to winter as the ambient temperature is higher in summer which increases the PV cell temperature thus reducing the electrical output.

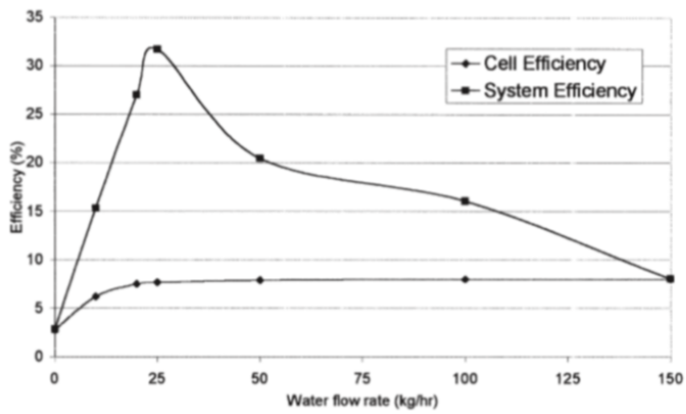

Figure 2.6: System(total) efficiency and cell(electrical) efficiency of the PV-T with increasing flow rate, obtained by Kalogirou . [25]

Prakash developed a mathematical model to predict the performance of a PV-T module of design as seen in Figure 2.7, with varying reservoir depth and flow rates. The electrical and thermal efficiency is highest for a lower depth of the reservoir and a higher flow rate. For a depth of 1 cm and a flow rate of 120 kg/h, the total efficiency was 76% whereas for a depth of 3 cm and flow rate of 40 kg/h, total efficiency was 59% [34].

Tiwari and Sodha modelled four combinations of the PV-T design- glazed and unglazed, and with and without a Tedlar back sheet, (Figure 2.8) to study their annual performance for the location of New Delhi, India [48]. The unglazed without Tedlar back sheet type showed to have higher thermal efficiency as the heat from the cells is directly transferred to the water below it. The thermal efficiency reached 65% in summer and 77% in winter. The higher efficiency in winter is due to lower heat losses from the PV-T surface in winter compared

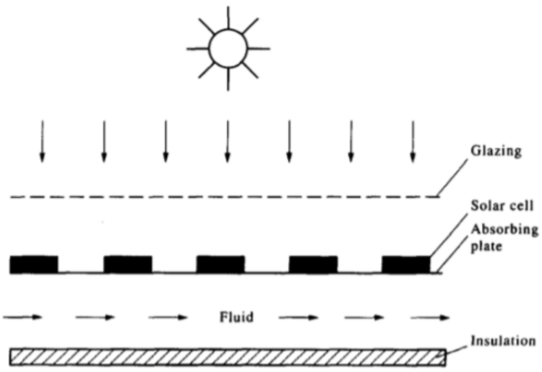

Figure 2.7: PV-T design used by Prakash for its performance study. [34]

to summer. Tests for increasing flow rates indicated that the total system efficiency increased whereas the outlet water temperature decreased.

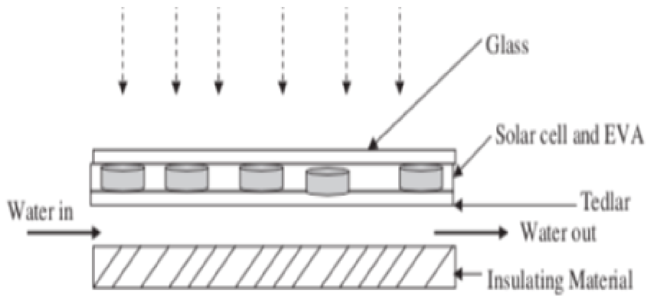

Figure 2.8: PV-T design used by Tiwari and Sodha for the performance study in New Delhi. [48]

In the study by Cen, water is in direct contact with the PV panel thus eliminating the need for metallic tubes for water flow and thus reducing the costs of the PV-T module. The highest electrical efficiency of the PV-T module was obtained with a bifacial PV panel of 13.4% followed by 12% with a monocrystalline PV. As mentioned previously, the thermal efficiency obtained was 53%. It was also observed with varying depth of the reservoir that a shallow reservoir takes less time to heat up thus yielding higher outlet temperatures compared to a deeper reservoir [6]. The direct contact between water and the panel and reduction in tubing make the design a technically and economically viable option for use in desalination, as high outlet temperatures and quantity of water can be achieved.

2.2. Desalination Technology

Desalination plants require a large amount of energy to produce freshwater from seawater and brackish water. The system consists of an input feed of water to be desalted and two output streams, one of the freshwater and one of waste brine [35]. Solar energy can be used to produce the energy required for desalination. It can provide the electrical energy requirement of the desalination plant or/and provide thermal energy for the plant's input requirement [24]. Solar desalination can be classified into direct and indirect solar desalination.

In Direct solar desalination, the distillate is produced directly within the solar collector and has a low output product temperature. Direct solar desalination requires a large area for installation. Therefore, it is competitive to indirect desalination only for applications where the demand is less than 200 m^3/day [35]. The advantage of this method is the simplicity of design and low operational costs.

The indirect solar desalination combines the PV-T system or conventional solar collectors with conventional desalination technologies. The heat produced by the collectors can be used to preheat seawater for desalination and to generate steam for use as input to the thermal desalination processes [20]. The steam can also be used to generate electricity for the plant requirement [32]. The benefit of using the PV-T technology is that it can provide both, the heat required for the plant input as well as generate electricity for the plant requirement without any losses that are encountered in electricity generation using steam turbines. The productivity of indirect desalination plants is 10 to 20 times greater than that of direct desalination plants for the same area [13]. The indirect method produces about 60 l water per m^2 per day as compared to 4 l of water per m^2 per day by the direct desalination method [35]. Therefore, a land area of 50,000 m^2 is required to produce about 200 m^3 of water by direct desalination.

The commonly used conventional desalination processes are classified into phase change or thermal processes, and membrane processes. The phase change/ thermal processes are the Multi-Effect Distillation (MED), Multi-Stage Flash Distillation (MSF) and Vapour Compression Distillation (VC). The membrane processes are Reverse Osmosis (RO) and Electrodialysis (ED). The MED, MSF and VC processes require thermal energy as heat input and electrical energy for the pumps and other auxiliaries in the system. RO and ED require electrical energy for the desalination process.

2.2.1. Solar stills

The solar still is a type of direct solar desalination process (Figure 2.9). It converts solar energy to thermal energy as well as produces distilled water. The solar still is constructed by covering a basin consisting of saline water with a transparent sloping glass cover. The heat of the incoming solar irradiation is trapped in the water which thus heats up causing it to evaporate. The water vapour is condensed on the inner sliding cover and freshwater is collected at the sides [13]. Since condensed vapour is collected, all the compounds are left behind in the basin giving high-quality water. About 3-5 l per m^2 per day water can be produced by the solar still, its efficiency being up to 35% [24, 35]. The disadvantage of the solar still is that a layer of sludge forms at the bottom of the basin which needs to be cleaned regularly. Certain improvements can be made to the design which includes adding a double glass cover instead of single pane glass, adding black dye in the water to increase heat absorption, adding a stream of cooling water between them to increase the temperature difference between the water in the basin and the cover, thereby increasing the condensation [24, 35].

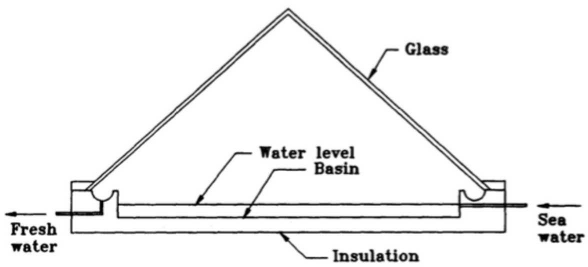

Figure 2.9: Schematic of a solar still. [24]

2.2.2. Multi-effect Distillation

The Multi-effect Distillation is one of the oldest and well-established desalination technologies, first used in the 19^{th} century [51]. (Figure 2.10). It involves multiple effects (stages) in which seawater is evaporated. This vapour is transported to the next effect where it is used to evaporate seawater by condensing. Each subsequent effect has a lower temperature with a minimum of 5^{o} C difference, and pressure than the preceding effect. The heat (steam) required for evaporation in the first effect is provided by the employed solar technology. The heat from this steam transfers heat to the seawater stream wherein it evaporates leaving product brine at the bottom of the first effect. The input steam, the vapour produced and the brine is then transferred to the next effect, and so on. The heat input to the first effect should be around 60- 70^{o} C for a MED plant, the maximum temperature of the first effect being 120^{o} C to prevent scaling [30, 51]. It requires 1.3 kWh electrical and 48.5 kWh heat input per m^3 of distilled water produced [30]. Therefore, electrical energy from renewable energy sources and low-cost waste heat must be considered.

As there is a contact between steam and the brine, the MED vessel that is in contact with seawater or brine could be prone to corrosion. With appropriate materials like stainless steel and titanium for the plant design, the MED plant life can be about 40 years [51]. Therefore when the initial costs are higher, the lifetime of the plant is higher.

A solar-powered MED desalination plant in Gaza, which used electrical energy from PV and heat from solar collectors yielded between 6 to 13 l of water per m^2 per day. The performance ratio (PR) which is the amount of distilled water produced (kg) per 2326 kJ is between 12 to 14 for MED [3, 49].

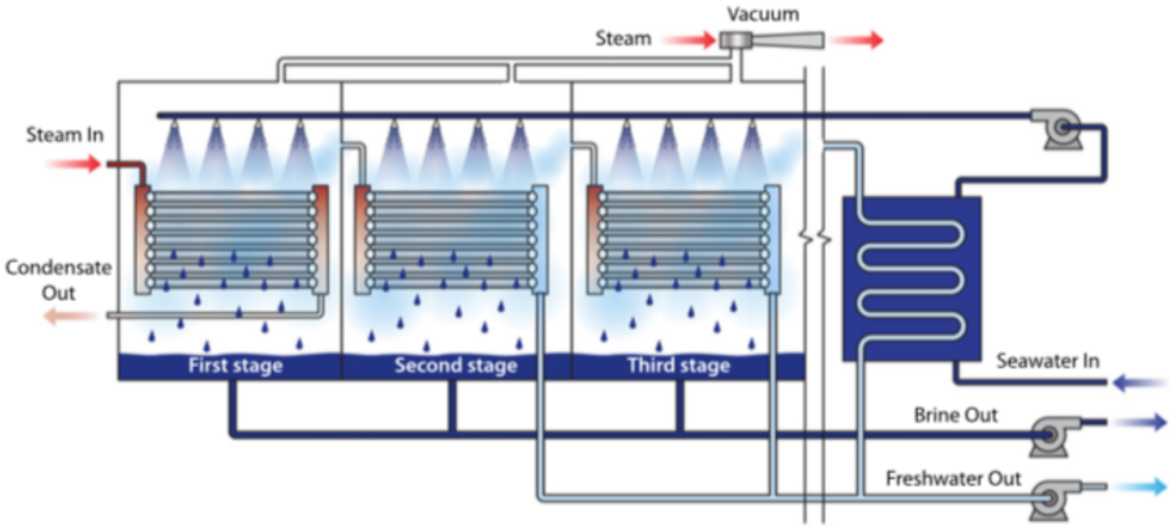

Figure 2.10: Illustration of the multi effect distillation (MED) process. [3]

2.2.3. Multi-stage Flash Distillation

The MSF technology is another most commonly used desalination technology is terms of its capacity, since the early 1960s [24, 51]. Like the effects in the MED, the MSF consists of flash chambers called stages where seawater is flashed in each chamber at a lower pressure than that of the preceding chamber, to generate vapour, as seen in Figure 2.11. This vapour is condensed by a series of pipes where the seawater is preheated. The input temperatures required for MSF desalination are 80 to 90^o C and thus require more energy over MED desalination [20]. Scaling is an issue in MSF processes due to the flashing of steam, therefore regular cleaning is required [3]. A solar-powered MSF plant can produce up to 6- 60l of water per m^2 per day. The performance ratio for MSF desalination is usually between 6 to 10 [24].

2.2.4. Vapour Compression Distillation

Vapour Compression has a similar principle to that of MED, only that the heat required for evaporating seawater is generated by compression of the vapour instead of condensation [51]. A Mechanical Vapour Compressor (MVC) or a Thermovapour Compressor (TVC) is used for this vapour compression [49]. The heat from this vapour is then used for the further evaporation process. As the vapour pressure rises, the condensation temperature rises as well, thus this can be used as the heating medium for the same stream from which the vapour was produced. The seawater stream extracts heat from this vapour thus producing distilled water whilst generating more steam. The size of a VC plant is limited by the availability of the compressor capacity. From cost study analysis, VC distillation is not economical as a stand-alone design [24]. It can be used in combination with MED to recover the latent heat of vapour [24, 49]. The process schematic is seen in Figure 2.12

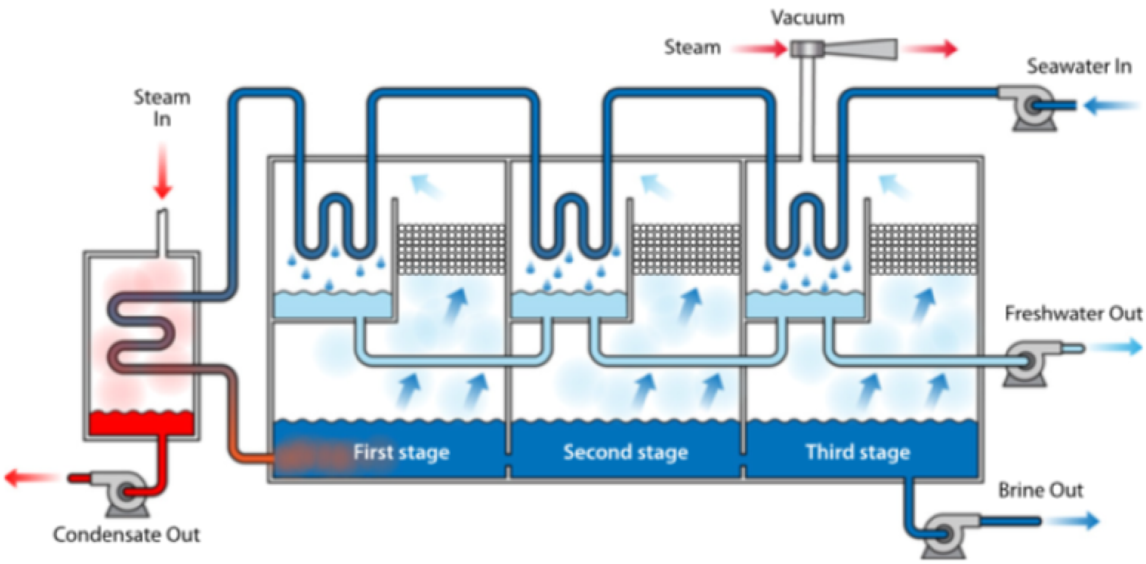

Figure 2.11: Illustration of the Multistage flash (MSF) process. [3]

.

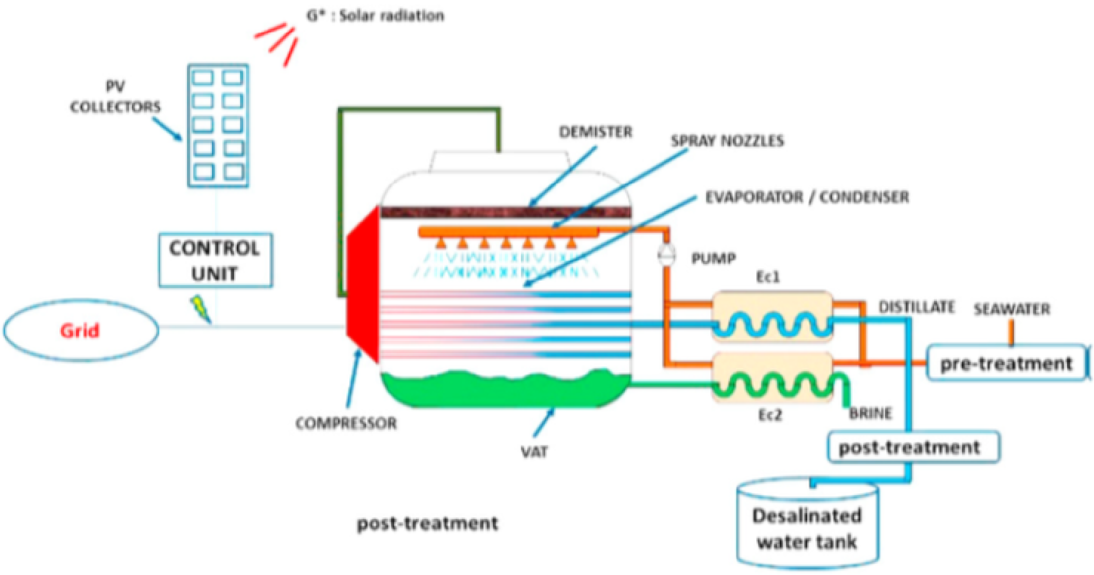

Figure 2.12: Illustration of the vapour compression (VC) process. [49]

2.2.5. Reverse osmosis

The first RO application was back in the 1960s for brackish water intake. Seawater desalination became possible within the later years with the first plant being installed in the year 1981 [13, 51]. A semipermeable membrane is used wherein seawater enters at a pressure of 50 bar, which is higher than the seawater osmotic pressure (27 bar) [24]. Due to the high-pressure, water flows through the membrane leaving behind salts and other compounds on the other side of the membrane (Figure 2.13). A high-pressure pump is required to pressurize this feedwater. The disadvantage of RO is fouling of the membrane over time when the salt density index is high [51]. Therefore, pretreatment of water is required before it can come in contact with the membranes. Although only water can pass through these membranes, some tiny particles of salt may still pass through water on the other side. To avoid this a higher water pressure is required which further increase the energy consumption for the process. Also, this freshwater still contains microbes. A post-treatment is therefore required to remove these as well as to adjust the pH levels [49].

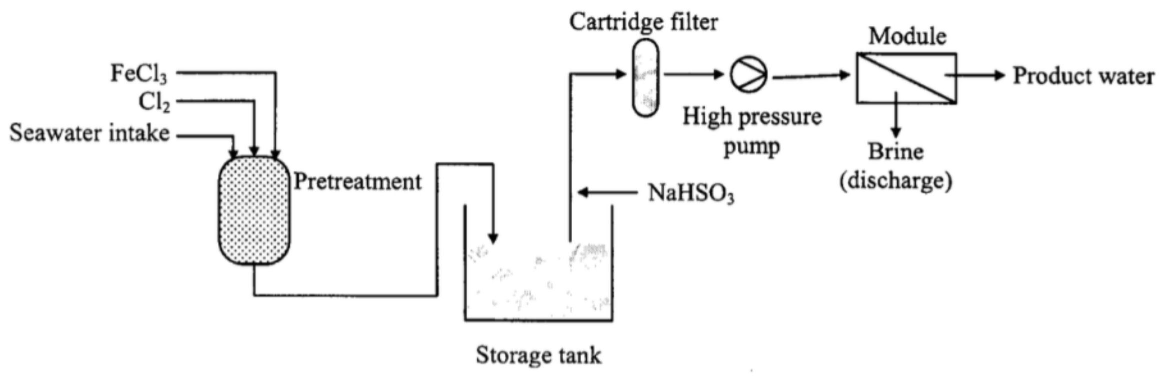

Figure 2.13: Reverse osmosis (RO) process. [51]

2.2.6. Electrodialysis

Electrodialysis is the process of using an electric potential to form a cationic and an anionic membrane so that a diluted freshwater and salt stream can be obtained from seawater, as seen in Figure 2.14. The salts contain sodium and chlorine ions which are positively and negatively charged respectively. These move towards the electrodes that have opposite charge, thus leaving water without any salts in between the electrodes. The cost of ED depends on the number of dissolved salts, therefore, it is only feasible when the concentration of salts is not more than 6000 ppm, and thus is not economical for seawater desalination [24]. Also, as water has a low conductivity, ED cannot be performed on the water which has a salt concentration of less than 400 ppm [24].

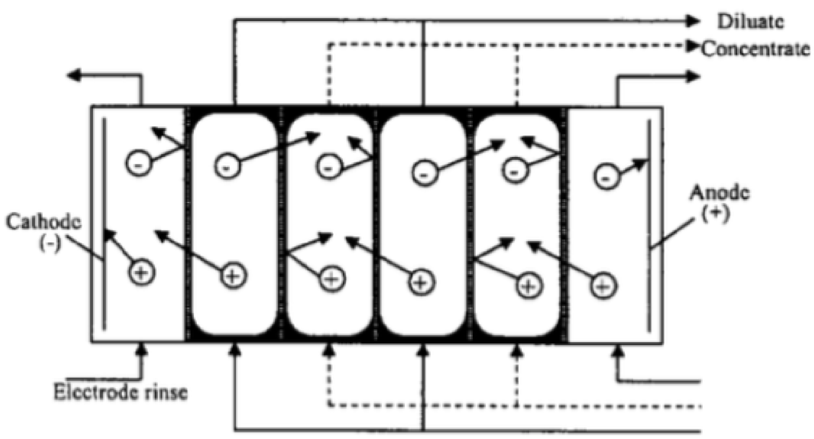

Figure 2.14: Electrodialysis (ED) process. [51]

2.2.7. Overview of technologies

The selection of technology for a solar desalination plant depends on its compatibility with solar technology, the energy requirements, pre- and post-treatment requirements, the plant performance and the capital and operating costs [24]. MED is more suitable to combine with PV-T as it requires low operating temperature and pressure inputs over the MSF process. Due to lower input temperature, the effects of corrosion and scaling are also reduced compared to MSF, and, the PR of MED (12-14) process is higher than that of MSF (6-10). Another advantage of the MED process is that it can be operated at a reduced capacity, making the coupling with solar technology efficient [18].

According to a survey by Kalogirou, [24], the energy requirements for RO are the lowest with 144 kJ/kg compared to 149 kJ/kg for MED, however, RO requires water treatment before and after the process, thereby making it expensive compared to MED. Also, the distillation process is preferred over membrane processes as it kills any microbes in the process, giving safe water.

The efficiency of MED plants can be increased by combining it with the MVC system [45]. The latent heat of condensation in the MED process can be recovered by the MVC to further increase the evaporation [16]. **The MED-MVC specific power consumption is similar to that of RO-6-8 kWh/m^3 and the reliability of this system is higher in comparison to RO with a value of 90% [45].**

3 Solar powered desalination plant

This chapter describes the design of the novel PV-T powered MED with MVC technology. The PV-T design aims maximum extraction of the thermal energy which is then stored in an insulated tank. This hot water is then flashed in a flash vessel at a low pressure to produce steam, which is used as an input to the first effect of the MED vessel. The steam from the last effect of the MED is compressed by the MVC which increases its heat enthalpy to be used in the first effect of the MED. The electrical energy produced by the PV-T panels is used for the electrical requirements of the plant. Excess energy produced is stored in batteries which enables the plant to run even at night-time. The subsystems of the plant are seen in Figure 3.1 and are explained below.

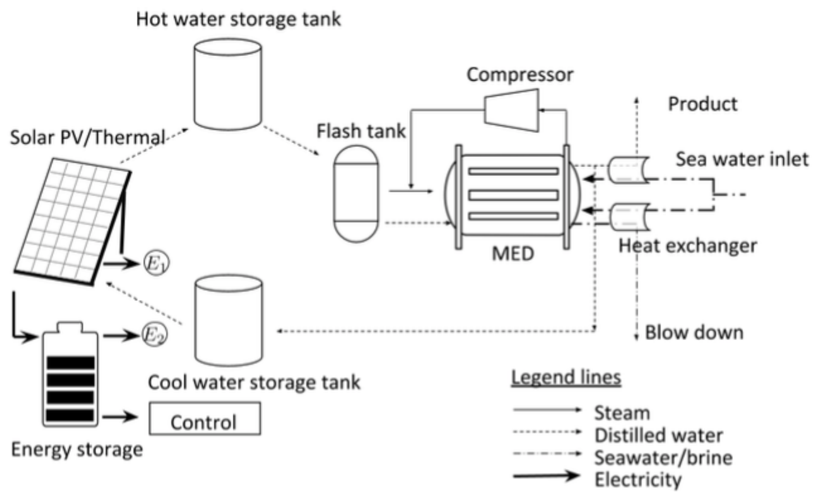

Figure 3.1: Main components of the solar powered desalination plant. [15]

3.1. PV-T Panel

The PV-T panel uses a standard PV panel to which a thermally insulated water reservoir is attached. The water flows across the surface of the PV panel, extracting heat from it. The panel has an inlet and outlet, each with a direct solenoid valve and temperature sensor, placed diagonally to each other. The panel is tilted with its inlet near to the ground (see Figure 3.2). Distilled cold water flows in through the inlet towards the outlet whilst extracting heat from the PV panel. The temperature at the outlet can be set to the desired target water temperature for automatic control of flow to the panel. A control system is set up to allow for manual and automatic management of flow and for recording temperature data. Thus, the valves automatically open when the set temperature is reached and hot water flows out through the outlet while cold water enters the reservoir through the inlet simultaneously, following the thermosiphon principle. Hot water of up to 90^{o}

C can be produced which is stored into the hot water tank. 400 such PV-T panels placed at a south-west orientation, form the PV-T array in the plant.

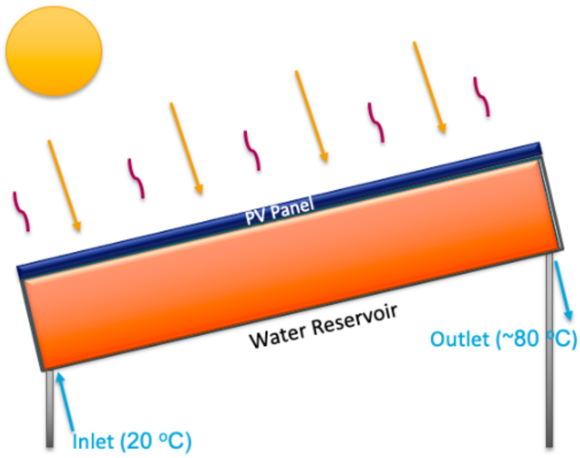

Figure 3.2: PV-T module working principle.

3.1.1. Panel design (This section is confidential)

3.2. Electrical and Thermal storage

The electrical and thermal storage for the PV-T array enables continuous production of distilled water from the plant.

3.2.1. Battery system

The excess electrical power generated by the PV-T array is stored in batteries and used for the plant auxiliaries, pumps, MVC, etc., during lower solar irradiation levels. The sizing of the battery storage system required for the plant has an impact on total system costs [23, 31, 42]. Therefore, it is necessary to initially reduce the electrical requirements by optimising the plant design.

To reduce pump requirements, gravity-fed tanks and equipment are used wherever possible. The delivery pressure in the plant is below 6 bar, therefore low power pumps are used.

3.2.2. Storage tanks

Cold water tanks are used to store distilled water for the PV-T array. Insulated hot water tanks are used to store water heated by the array for later use in the flash vessel and the desuperheating requirements of the vapour compressor. Desuperheating prevents the fluid under process in the MVC from superheating, thereby protecting the equipment. The cold-water tanks are installed at a height well above that of the PV-T panels so that water flows in the panels through gravity, without additional pumping power.

3.3. Thermal Energy Inputs

The thermal energy (i.e. steam) input to the MED vessel is provided by the flash vessel and the mechanical vapour compressor.

3.3.1. Flash vessel

Saturation pressure of water is the pressure at which liquid water and its steam are in thermodynamic equilibrium. When the pressure of water drops below its saturation pressure, all the heat cannot be retained in liquid form, thus converting the excess heat to latent heat of vaporization [43]. This is known as flash evaporation or flashing. The water stored in the hot water tanks flows to the flash vessel by a difference in pressure. The hot water is stored at atmospheric pressure, ~1 bar whereas the flash vessel is at a pressure of 0.2 bar where hot water evaporates under low pressure to generate steam. This is then used as an input to drive the first effect of the MED.

3.3.2. Mechanical vapour compressor

The vapour from the last effect of the MED is compressed by a mechanical vapour compressor to raise the vapour pressure equal to that of the required input pressure of the first MED effect. This vapour is then fed back to the first effect as an input along with steam from the flash vessel. Thus, the MVC recovers the energy in the low-pressure vapour by compressing it to the same conditions as in the first effect resulting in a low volume and high temperature and pressure vapour.

3.4. Multi-Effect Distillation vessel

The Multi-effect distillation process, as discussed in the last chapter, consists of four stages called effects which have a decreasing temperature and pressure in each effect. Each effect has horizontal tube bundles carrying steam produced by the flash vessel and the mechanical vapour compressor. Seawater is sprayed on these tube bundles where it flows down by gravity, leaving a thin film of seawater over it [12]. This thin film partially evaporates due to heat transfer from the tubes. Thus, a stream of brine is created at the bottom of the effect and a vapour stream at the top, which is then used as a heating medium for the following effect.

The vapour is transferred to the next effect after passing through a demister which prevents any brine droplets transferring along with the vapour. The brine stream is transferred to the next effect due to pressure difference between the two effects. The temperature of the brine is reduced to that of the next effect due to evaporation of the brine at lower pressure. This brine transfer to the next effects helps in minimizing scaling as the highest concentrated brine goes into the last effect where it is exposed to the lowest temperature, and eventually drained to be disposed of.

The distilled water from each effect is drained as product water. Some of the product water is siphoned off and stored in the cold-water tank to be supplied to the PV-T array.

The minimum temperature of the first effect must be 55^o C considering that the temperature in the last effect cannot be lower than 40^o C due to the temperature of incoming seawater.

4

Thermal Model

The modelling tools and the theory used for the performance prediction of the PV-T panel will be described in this chapter.

4.1. Buckingham's Pi Theorem Analysis

The heat transfer in fluids can be characterized by coupling heat and flow equations. Generally, the process is described by a set of continuity, momentum and energy conservation equations. These involve physical quantities that represent properties of the material and the surrounding medium [54]. The intensity of coupling is represented by the magnitude of these physical quantities which correlate according to the laws of physics. The units of these physical quantities can be expressed in terms of combinations of fundamental units of mass, length, time and temperature. Using Buckingham's pi theorem analysis, these independent parameters can be coupled together to form dimensionless groups [37]. The procedure is as follows:

1. List the involved parameters
2. Write them in the form of fundamental dimensions
3. Choose the repeating variables
4. Evaluate pi terms
5. Determine the final equation

The ΔT, temperature difference between the fluid outlet temperature and inlet temperature is given by,

$$\Delta \mathrm{T} = \mathrm{f}(\mathrm{q}, \rho, \mu, \mathrm{k}, \mathrm{Cp}, \mathrm{v}, \mathrm{l}) \tag{4.1}$$

where, q = heat flux on the panel (W/m^2) :[J L^{-2} T^{-1}], ρ = density of fluid (kg/m^3) :[ML^{-3}], μ = dynamic viscosity (Ns/m^2) :[M L^{-1} T^{-1}], k = thermal conductivity (W/mK) :[J L^{-1} T^{-1} θ^{-1}], Cp = specific heat capacity (J/kgK) :[J M^{-1} θ^{-1}], v = inlet velocity of fluid (m/s) :[LT^{-1}] and l = hydraulic diameter (m) :[L]

There are 8 variables (n) and 5 fundamental dimensions (m) involved; therefore, there will be n-m = 3 dimensionless groups. Selecting repeating variables and applying the pi theorem, the dimensionless correlation is,

$$\Pi_1 = C(\Pi_2, \Pi_3) \tag{4.2}$$

$$\Pi_1 = \Delta T / q^{\mathrm{a}}, \rho^{\mathrm{b}}, \mu^{\mathrm{c}}, k^{\mathrm{d}}, l^{\mathrm{e}} \tag{4.3}$$

$$\Pi_2 = v / q^{\mathrm{a1}}, \rho^{\mathrm{b1}}, \mu^{\mathrm{c1}}, k^{\mathrm{d1}}, l^{\mathrm{e1}} \tag{4.4}$$

$$\Pi_3 = C_p / q^{a2}, \rho^{b2}, \mu^{c2}, k^{d2}, l^{e2} \tag{4.5}$$

Solving equations 4.3, 4.4, 4.5,

$$\Pi_1 = \Delta T k / q l \tag{4.6}$$

$$\Pi_2 = v \rho l / \mu \tag{4.7}$$

$$\Pi_3 = C_p \mu / k \tag{4.8}$$

Therefore, from 4.2, 4.6, 4.7, 4.8,

$$\Delta T k / q l = C(v \rho l / \mu, C_p \mu / k) \tag{4.9}$$

ql/kΔT , v ρ l / μ and C_p μ / k are defined as the Nusselt, Reynolds and Prandtl numbers respectively.

Thus,

$$\Delta T = q l / k^{*} C(Re, Pr) \tag{4.10}$$

The equation states that the temperature difference between the inlet and outlet of fluid can be obtained based on the irradiance values, type of inlet fluid and its velocity, and the reservoir dimensions, which will be verified with experimental and simulation data in the next chapter.

4.2. Modelling Approach

The approach to developing the PV-T model to perform predictions and sensitivity analysis is as described below and seen in Figure 4.1.

1. Meteonorm is used to obtain hourly weather data for the location, which includes irradiance, temperature and wind speed parameters [33]. These values and the PV Module specifications from the datasheet- electrical, geometrical, temperature coefficient, are given as an input to the PVMD Toolbox to calculate the electrical yield of the module and module temperature. The PVMD Toolbox, hereafter called the Toolbox, is a tool developed by the PVMD Department of the Delft University of Technology (TU Delft), to predict the yield of a PV module [19].

2. Heat sources within the layers of the PV-T module are calculated using Genpro4. The GenPro4 software is an optical model, combining ray optics and wave optics [41].

3. A model of the PV-T panel with all the layers is developed in COMSOL Finite Element Method software. Heat input to the model is given by subtracting the electrical yield calculated using the Toolbox from the heat sources calculated by GenPro4. The output from the COMSOL model is a temperature gradient across the panel volume and the layer surface.

4. The temperature of PV cells in the COMSOL model accounts for the effects of flowing water on the cells. Comparing this with the temperature of the module from Toolbox (which does not take into consideration the effects of flowing water), and using the temperature coefficient of the module, a new corrected value of electrical yield is obtained.

5. The new value of heat input to the COMSOL model is calculated using this yield, and the final temperature gradient is obtained.

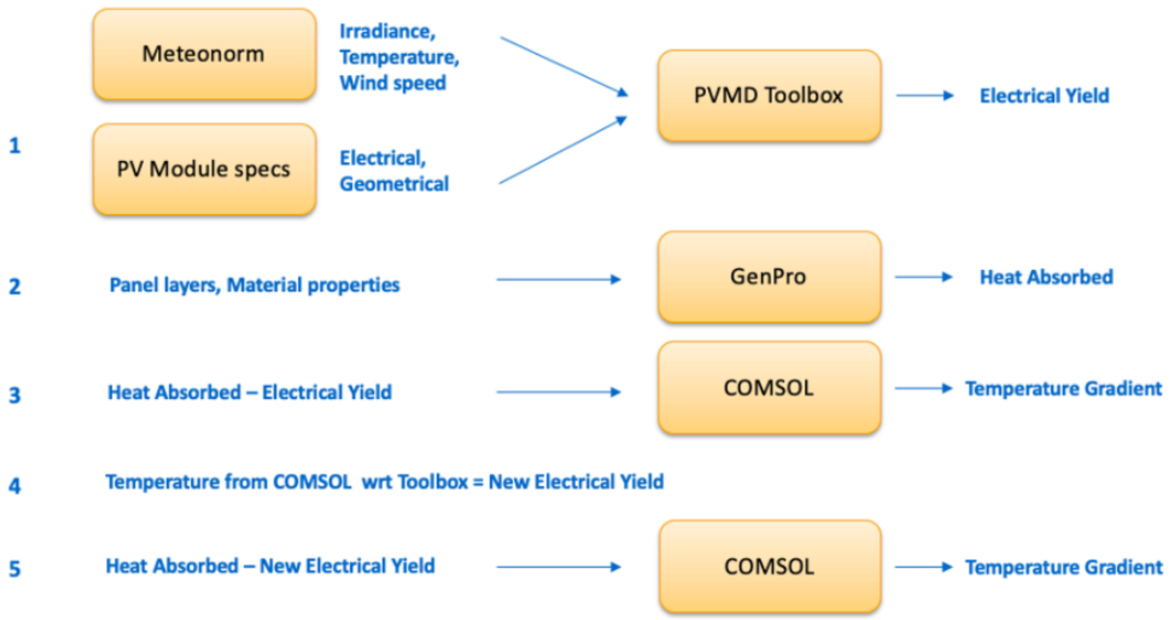

Figure 4.1: Modelling approach followed.

4.2.1. Definition of heat sources

The heat sources within layers of the panel must be defined to predict the thermal energy absorbed by the fluid. The irradiance absorbed by the PV module, that is not converted to electricity accounts for heat, which increases the temperature of module [21].

GenPro4 is an optical model that calculates the light reflectance, absorptance and transmittance (R, A, T) with respect to the wavelength for a cell [41]. Thus, the fraction of incident light absorbed in each layer, by taking scattering and light trapping into account, is calculated. This is known as the absorption factor. The material layers, thicknesses, their refractive indices and extinction or, absorption coefficient as a function of wavelength need to be specified as inputs.

The layers of the panel and the thickness of each layer is defined in the software as seen in the previous chapter (Section 3.1.1). Aluminium back contacts of the PV module are not taken into consideration for simplifying calculations. Simulation for a wavelength range of 200 to 2000 nm has been performed and the results are obtained as seen in Figure 4.2(a). From the plot, it can be observed that the maximum absorption is in the silicon layer, followed by water. Silicon absorbs the part of the spectrum from 250-1200 nm [46]. The white air layers correspond to the reflection and transmission from the front and rear surface of the module.

The absorption factor (A) for each layer is calculated using 4.11, where A(λ) is the absorption value w.r.t the wavelength and G(λ) is the AM 1.5 spectrum [40]. The absorption factor of the solar cell affects the thermal efficiency of the PV-T module. When the silicon absorption factor increased from 0.7 to 0.9, the thermal efficiency increased by 8% [40].

$$A = \frac{\int A(\lambda) G(\lambda) d\lambda}{\int G(\lambda) d\lambda} \tag{4.11}$$

Part of the PV cells is covered by the busbars and fingers which form the metal grid. This must be taken into account for calculating the absorption in the cell layer. This is done by,

$$A_{\text{cell}} = A_{\text{a}} a_{\text{a}} + A_{\text{grid}} a_{\text{grid}} \tag{4.12}$$

where A $_{\text{a}}$, a_{a} are the values of absorption and area of the active area of cell and A $_{\text{grid}}$, a_{grid} are the values of absorption and area of the grid [21].

The values for the absorption and area of the grid are taken from literature. The spacing between cells is not taken into consideration for ease of calculations.

For the PV layer, the efficiency value of the PV module is subtracted from the total absorption factor to account for the electricity produced from the absorbed irradiance. This efficiency is calculated using results from the Toolbox. The part of the AM1.5 spectrum absorbed by the layers is seen in Figure 4.2(b). The absorption factors calculated by the above approach can be seen in Table 4.1.

Table 4.1: Absorption factors of module layers.

Layer	Absorption factor (%)
Top glass	2
Top glass PV	0.7
EVA	1
Silicon	$52 - \eta_{PV}$
Water	10
Bottom glass, Al, foam	Negligible

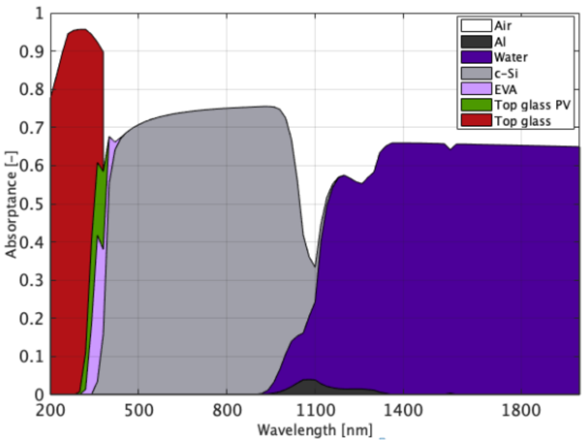

(a) Fraction of the solar spectrum reflected, transmitted and absorbed in each of the module layers.

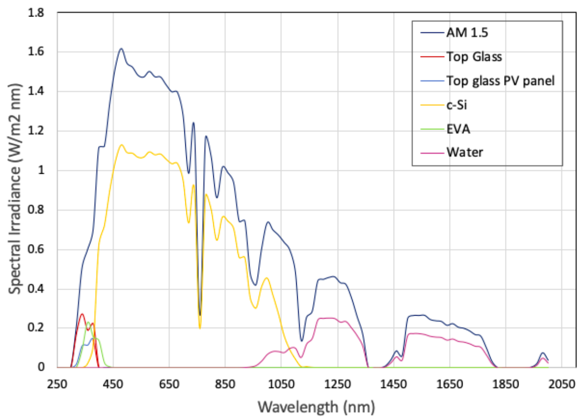

(b) The AM 1.5 spectrum with spectral absorption in layers of the module.

Figure 4.2: Absorption values for the PV-T module configuration.

4.2.2. Location weather data

Meteonorm v 7.2 software is used to obtain hourly weather data including the parameters of ambient temperature, wind speed, Global horizontal irradiance (GHI), Diffuse horizontal irradiance (DHI), Direct normal irradiance (DNI) and the altitude and azimuth of the sun. Location coordinates and the site altitude, orientation and inclination of the panel, site albedo and the site horizon are given as inputs. If the custom location of the site is not available, a user-defined location is created using the coordinates. Therefore, the coordinates and the altitude for the site in Dubai are used. Meteonorm uses measured values from nearby locations to compute weather data for the specified custom location. For the location of Dubai, the panels are facing South-West and, South for West Bengal.

A horizon profile of the site can be created in order to include the effects of the profile on the hourly values. A picture of the horizon can also be inserted as an input. A custom horizon for Dubai is thus created (Figure 4.3) based on a panoramic picture of the site as seen in Figure 4.4.

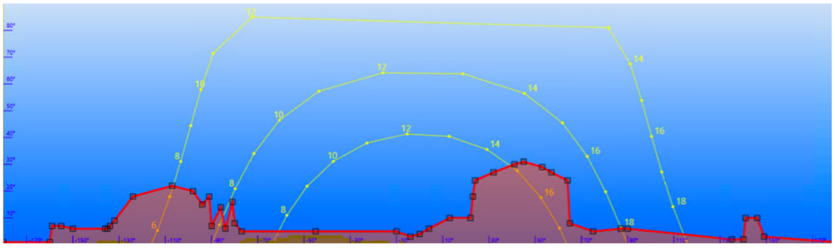

Figure 4.3: Horizon of the Dubai site created in Meteonorm.

Figure 4.4: 360^{o} image of the site in Dubai.

4.2.3. Calculation of electrical yield

The PVMD Toolbox is used to calculate the electrical yield of the module. It consists of four sub-modules: Cell, Module, Weather and Electric. (Figure 4.5)

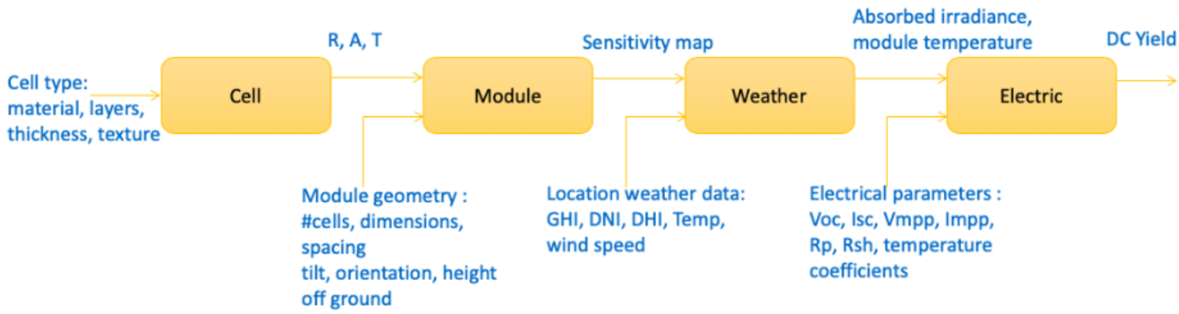

Figure 4.5: Sub-sections of the PVMD Toolbox.

1. Cell: The cell block calculates the angle of incidence dependent and wavelength-dependent reflectance, absorptance, and transmittance of light, for the selected cell type. GenPro4 model is used to calculate these values.

2. Module: The module block takes the geometry and surroundings of the module into consideration to model its effects. It requires the number and dimensions of cells and, spacing, the thickness of the module, module tilt, orientation, and, height from the ground as input. The surrounding geometry of the module i.e, the front and side distance between the modules is also required to account for mutual shading between them. These, combined with the output from the Cell block give a sensitivity map which is the sensitivity of the surface to incident light based on the angle of incidence [39].

3. Weather: The weather block requires the site-specific meteorological data as input and combines it with the output of the module block to calculate the absorbed irradiance by the module and its temperature.

4. Electric: The electric block gives the DC yield as the output based on the single diode model [46]. The input to this block are the module electric properties, Voc, Isc, Vmpp, Impp, and the temperature coefficients.

The energy yield for a summer day and winter day for the location of Dubai and West Bengal is calculated. Efficiency values are calculated from this which are used to finally calculate the absorption factor of the silicon layer as described in section 4.2.1.

4.2.4. COMSOL Model

The objective is to develop a model which predicts the thermal performance of the PV-T module under varying conditions. The model is developed using COMSOL Multiphysics v 5.4 which is based on finite element method (FEM). Problems in physics are defined by partial differential equations, some of which cannot be solved analytically. Discretization of such equations can be solved by numerical methods. FEM is a numerical method which discretises the problem by dividing the geometry into smaller parts called elements. These elements are characterized by low order polynomials to solve the problem [10]. Thus, the more the number of these elements, the higher is the accuracy.

The advantage of COMSOL is the ease of coupling necessary physics and, an extensive material library allowing for definition of all the layers. The temperature gradient along the surface and between the layers can be studied taking heat losses into account.

The model geometry is built in COMSOL using the CAD interface feature. The materials from the COMSOL material library are assigned to all the layers with their relevant properties. Next, the Fluid Flow and Heat Transfer physics modules have been included in the model. Subsequently, these are coupled using the Non-isothermal flow coupling. Finally, boundary conditions are defined based on the physical scenario of the design.

- Geometry definition and selection of materials

  A 3D geometry as seen in Figure 4.6, of the PV-T panel, is built using the CAD interface of COMSOL. A model built in AutoCAD can also be imported and used. However, the former method is chosen since all the layers can be perfectly overlapped. The generation of mesh requires that all the layers are overlapped properly to avoid errors during computation [44]. Initially, the geometry was built using original dimensions 1655 x 990 mm, but due to large computational strain, a smaller model, with one-eighth of each side was built. The model with layers as described in section 3.1.1 was built.

  Next, materials are assigned to all the layers from the COMSOL material library. The required properties for heat transfer- thermal conductivity, heat capacity and density, as a function of temperature, are selected. To account for radiation losses, emissivity values are required for the front surface, which are taken from literature [17]. For glass, EVA and PIR foam the material properties are defined manually from literature [36, 52].

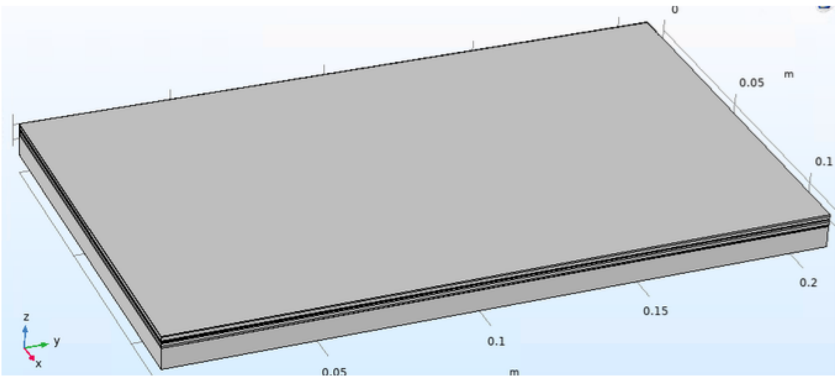

Figure 4.6: 3D Geometry of the PV-T module built in COMSOL.

- Generation of Mesh

  COMSOL Multiphysics has options of a physics controlled mesh and a user controlled mesh. The physics controlled mesh has element size options ranging from extremely coarse to extremely fine.

It builds the meshing sequence automatically w.r.t the geometry. A user controlled mesh can be built either by editing an already built physics controlled mesh and using the same sequence, or, by building a mesh from scratch by defining meshing sequence, element type, its size and distribution. For the former part, settings of individual mesh operations can be changed by adding sub-nodes to it or changing the element size [9].

Initially, a coarse physics controlled mesh was selected. But there were errors in computation due to the ratio between length, and thickness of layers. Also, the coarse mesh would give lesser accurate results. Choosing normal and fine element mesh gave a similar error. Creating a very fine mesh resulted in crashing of the file due to lesser computational capacity. Finally, fine element size physics controlled mesh was selected and editions were made to it by adding sub-nodes for the thickness of layers. The element size for the thinnest layers, (EVA and silicon) was given a value of one third the actual thickness of the layers. Mesh generation in the model is seen in Figure 4.7.

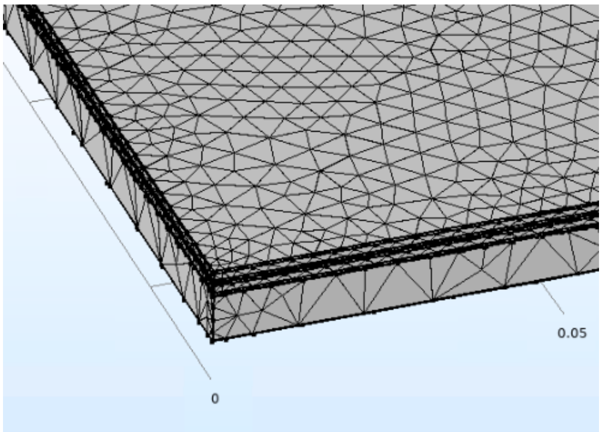

Figure 4.7: Generated Mesh in the module geometry.

- Heat transfer mechanisms

The next step is to add the heat transfer physics in the model. The model includes all heat transfer mechanisms of conduction, convection and radiation, which are involved in case of the PV-T module. These are explained below.

Conduction: Conduction refers to the transfer of energy between particles of a substance. The heat transfer across a medium exhibits a temperature gradient across it. As per Fourier's law, the conductive heat flux q is proportional to the gradient in temperature [8].

$$q_{\text{cond}} = -k\nabla T \tag{4.13}$$

Where k is the thermal conductivity of the medium.

Convection: Convection is the transfer of heat between a surface and moving fluid. It is defined by a heat transfer coefficient h, which is based on the fluid properties. Convective heat transfer can be forced or free (natural), or a combination of both. When the flow is forced by pumps, fans or atmospheric winds, it is termed as forced convection. Free or natural convection occurs due to the difference in density in fluid, that are caused by temperature differences. When both forced and free convection is involved it is termed as mixed convection. Convection effects are expressed by a ratio Gr/Re^2 [29] For Pr= 0.7, in case of aiding flow,

$0 < Gr/Re^2 < 0.3$ Forced convection
$0.3 < Gr/Re^2 < 16$ Mixed convection
$16 < Gr/Re^2$ Free convection

where Gr, Re and Pr is the Grashof, Reynolds and Prandtl number respectively.

The convective heat flux is proportional to the temperature difference between the surface and fluid as seen in equation 4.14. [5].

$$q_{\text{conv}} = h\left(T_S - T_f\right) \tag{4.14}$$

Where T_s and T_f are the surface and fluid temperature respectively.

Radiation: All surfaces at a non-zero temperature emit energy by electromagnetic waves. This radiative heat emitted is calculated by the Stefan-Boltzmann law given as equation 4.15 [5].

$$E = \varepsilon\sigma T_s^4 \tag{4.15}$$

Where ε is the Stefan-Boltzmann constant and σ is the surface emissivity.

- Physics Interface

The 'Conjugate Heat transfer' with 'Laminar flow' physics interface is chosen, which combines heat transfer in solids and fluids. Corresponding solid and fluid domains are assigned to them with their reference temperature. 'Non-isothermal flow' Multiphysics coupling interface is automatically added when the above interface is selected. It combines the effects of flow and temperature coupling. After necessary physics interfaces are added, boundary conditions are to be set based on heat transfer mechanisms discussed above. Conduction and convection heat transfer between the layers is accounted for by the inclusion of the chosen physics interface and does not have to be specified separately.

As discussed before, a fraction of incident irradiance is absorbed by the module. Heat is transferred throughout all the layers by conduction and convection (fluids) and the temperature of all the layers starts increasing as a function of the material thermal conductivity and heat capacity. Heat is also transferred to the surroundings via convection and radiation, termed as heat losses. This heat is lost via the top surface of the module. As stated earlier, the back surface of the panel consists of an insulation layer to prevent any heat loss. Heat loss through the sides is not included in the model as the sides are insulated.

Within the Conjugate heat transfer physics interface, individual heat sources based on values from section 4.2.1 are defined for all the layers using boundary conditions. The boundary condition for convective loss is defined for the top layer. COMSOL provides the option of either defining a heat transfer coefficient value or giving inputs for the type of convection, length, wind velocity and ambient temperature wherein the heat transfer coefficient is calculated. The latter is chosen in this case.

Radiation losses for the top layer are included using 'surface to ambient' boundary condition where ambient temperature and emissivity values need to be specified. Next, water inlet conditions of temperature and inlet velocity are defined using the temperature and inlet boundary conditions respectively.

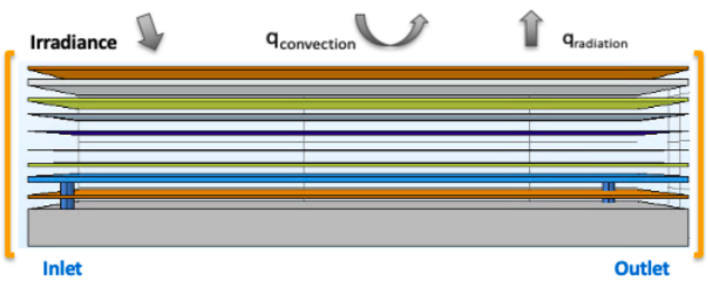

Figure 4.8: Heat exchange mechanisms defined in the COMSOL Model.

- Model inputs

Inputs to the model are weather data parameters- Irradiance, ambient temperature, wind speed, and, inlet velocity and temperature of the fluid. The parametric sweep option in COMSOL allows for the introduction of more than one combination of these parameters. The 'specified combination' type tests the parameter combinations as they are entered in the list. With the 'all combination' sweep type, it tests for a combination of all the parameter values with each other. The former option is chosen in this case.

The output from the model simulation is a temperature gradient across the layers and surface as seen in Figure 4.9(a). By additional post-processing tools, the average and maximum temperature of all and the individual layers can be obtained. The average temperature across the length of the reservoir can be obtained as seen in Figure 4.9(b). It is seen that the temperature of the water in the reservoir is higher (95^{o} C) towards the outlet. This is due to the inflow of lower temperature (20^{o} C) water from the inlet.

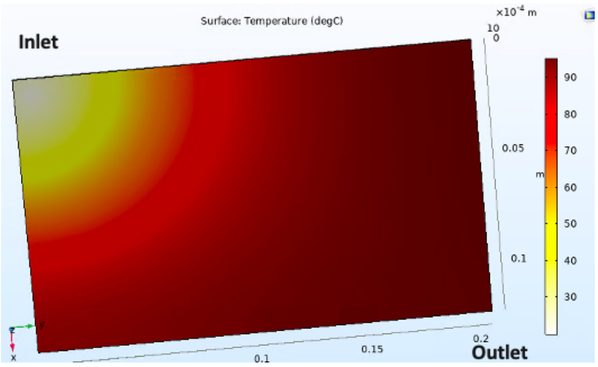

(a) Temperature gradient across surface from the COMSOL Model.

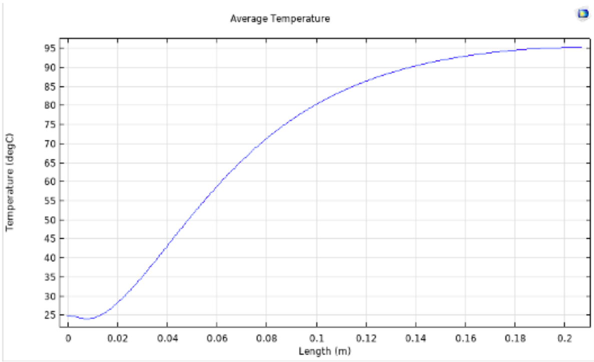

(b) Average temperature across reservoir length of module from inlet to outlet obtained from the COMSOL Model.

Figure 4.9: Output from the COMSOL model.

The model is validated using experimental test data from Dubai which will be seen in the next chapter. Simulations for varying irradiance, temperature and wind speed based on hourly values through the day (sunshine hours) are carried out to determine the outlet temperature profile throughout the day, for the two locations. Simulations were done for a summer and winter day. Inclination angles ranging from 0 to 28^{o} were tested. For each of these tilt angles, results for inlet velocity corresponding to the flow rates ranging from 0 to 80 l/h were obtained. The time taken by the simulation for an entire day (sunshine hours), for a combination of one tilt angle and flow rate was approximately 2.5 hours. Based on these results, contour plots for the optimum tilt and flow rate are made, as also seen in the next chapter.

5
Results

This Chapter presents the results obtained from the PV-T model, described in the previous chapter. Experimental results from test data and results from the COMSOL model are compared in order to validate the model. The model is then used to make thermal output predictions for the location of Dubai and West Bengal for different times of the year. Using data from these simulations, an equation describing the relation between the temperature difference of water at the inlet and outlet, and Nusselt, Reynolds and Prandtl number, as discussed in the previous chapter is derived.

5.1. Model Validation

To validate the thermal model, data from tests conducted in Dubai in September and October 2019 is used. These tests were conducted in order to analyse the most efficient way to harvest thermal and electrical energy and to test for the robustness of the current design.

5.1.1. Experimental Test setup

Three PV-T panels of the design described in section 3.1.1 were tested (Figure 5.1). The panels were mounted on a structure 1.2 m above ground level, with an inclination of 5^{o} facing South. Water flowed to the panels from a tank placed at a height 2.5 m above ground. The flow was controlled using direct solenoid valves at the input and output of the reservoir. Each panel was fitted with a control board for the management of flow based on a target outlet temperature and to record water temperature values. Hot water produced was collected to measure the yield of each individual PVT panel. The power output is recorded by the AP Energy Monitoring and Analysis (EMA) system.

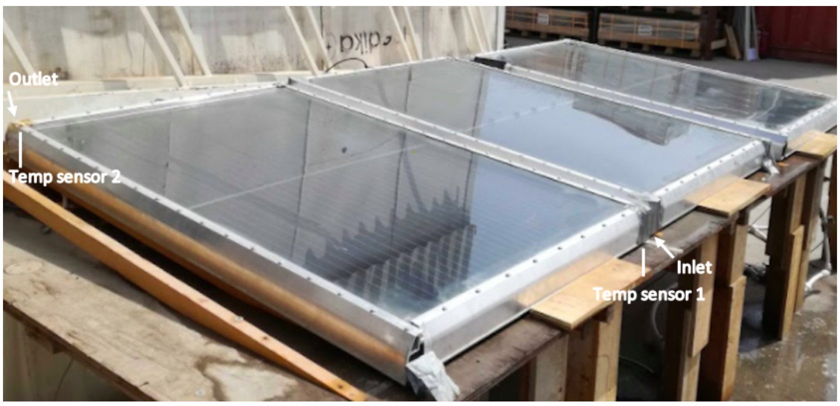

Figure 5.1: PV-T Test setup in Dubai, October 2019.

5.1.2. Experimental and simulation results

The results from the simulations and experimental data are shown below. Hourly values for weather data through the day (sunshine hours) were simulated. The Figures 5.2(a) and 5.2(b) display ambient properties on site for different days of testing. The blue curve indicates ambient temperature and the yellow curve indicates the irradiance values. Following Figures 5.3(a) and 5.3(b) display the experimental value of the water outlet temperature and the simulated outlet temperature values. The experimental values are displayed by dark blue markers with the yellow patch indicating thermometer error of +/- 2^o C, thus representing the range of temperature values of the outlet water. The simulated curve is displayed by a light blue solid line.

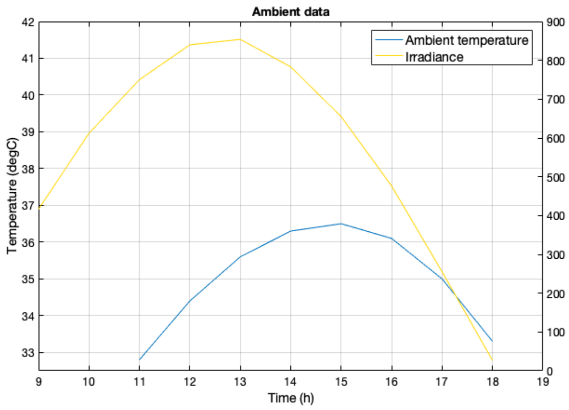

(a) Ambient data day 1

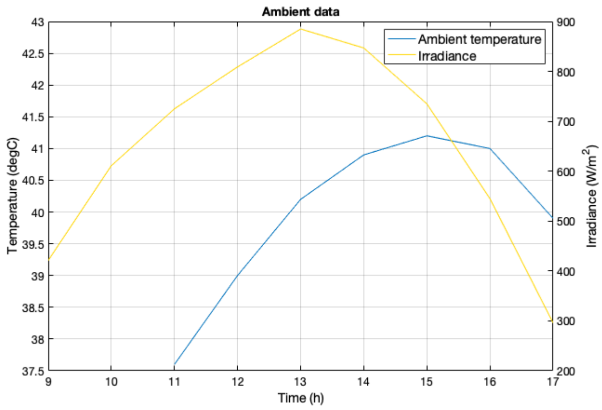

(b) Ambient data day 2

Figure 5.2: Ambient data for Dubai during testing.

Further, Figures 5.4(a) and 5.4(b) represent the experimental and simulated values of power output from the panel. Experimental values from test data are displayed by dark blue markers while the light blue solid line displays the simulated value from the model.

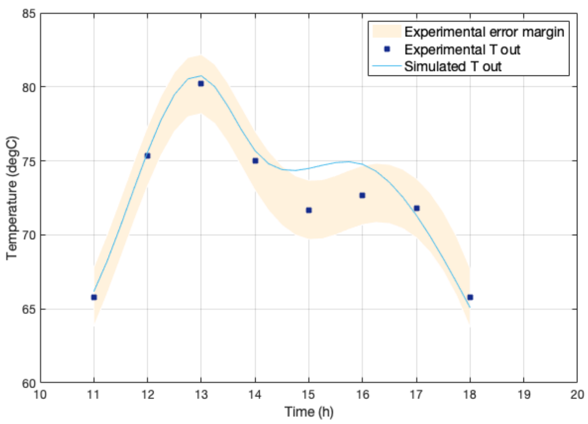

(a) Test Day 1

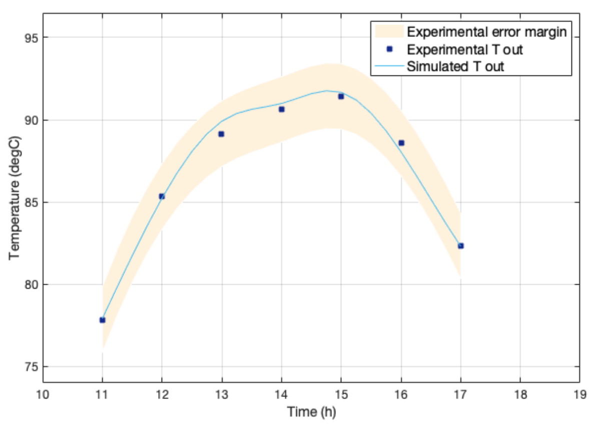

(b) Test Day 2

Figure 5.3: Experimental vs Simulated values for the outlet temperature.

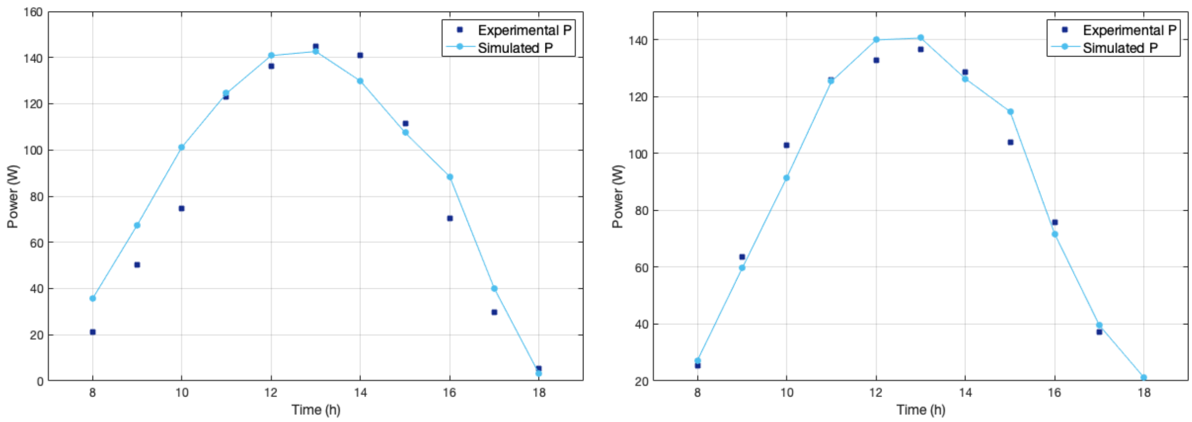

(a) Test Day 1

(b) Test Day 2

Figure 5.4: Experimental vs Simulated values for the power output.

The results present a good agreement between experimental data from site and simulated data from the model, as seen in Figure 5.3 and Figure 5.4. Majority of outlet temperature values from simulations fall within the error margin. The few higher temperature values, for instance, 2 pm to 4 pm for day 1 (Figure 5.3(a)) suggest higher convection losses at the site than the model calculated losses. Following this observation, a study concerning the effects of wind speed (convection losses) on the water outlet temperatures was done, which will be discussed further. Also, in the experimental model, the outlet temperature is set to a desired value. The water flows out of the panel as soon as it reaches this value. However, in the model, the temperature reaches a steady-state value, thereby suggesting a higher output temperature to what was set in the experimental panel.

5.1.3. Wind speed sensitivity study

A study to predict the effect of wind speed on water outlet temperature was done using the ambient data from Figure 5.2(b). This data was used as input along with a constant wind speed throughout the day as opposed to the actual varying wind speed. As seen in Figure 5.5, the outlet temperature is higher, with an average temperature in the day of 88^{o} C for a wind speed of 1 m/s, whereas it is lower (average temperature in the day = 80^{o} C) for a wind speed of 2 m/s. Thus, outlet water temperatures decrease with an increase in wind speeds due to higher convection losses. This data is especially useful for estimating the outlet temperatures achievable for a windy location or a location which is near to the coast.

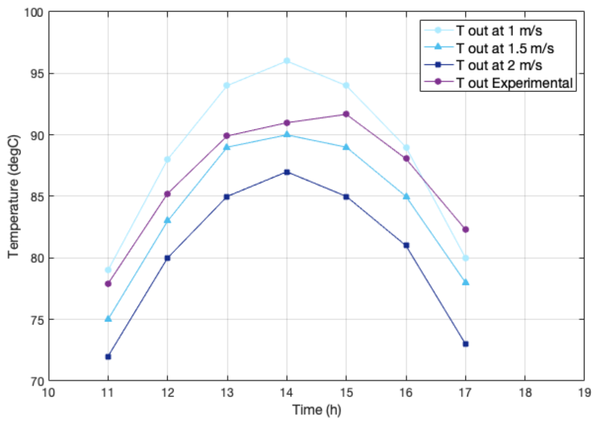

Figure 5.5: Effect of wind speed on the outlet temperature of water.

5.2. Results for the location of Dubai, UAE

The validated thermal model has been further used to predict the output from the PV-T panel for the location of Dubai. The aim is to find an optimum spot to maximize the quantity and temperature of hot water produced (to be used in the flash vessel) and thus extract maximum total (electrical + thermal) energy throughout the day. This is done by studying the effect of the volume flow rate of water through it and angle of tilt, on the water output temperature and obtaining optimum values for these parameters.

Predictions were done for a summer and winter day as explained in the previous chapter. Based on these results, contour plots for the average value of temperature difference between water inlet and outlet (T_out – T_in = ΔT) and total efficiency (η_{total}) were obtained. The total efficiency (electrical + thermal) as seen in equation 5.1 was calculated using equations 2.1 and 2.2 defined in Chapter 2.

$$\eta = \eta_{th} + \eta_{pv} \tag{5.1}$$

5.2.1. Summer day

The Figure 5.6 shows the ambient weather data for a summer day in Dubai, used for the simulations, and, the corresponding water outlet temperature (T_out) profile at a minimum flow rate and tilt, from the COMSOL model. Average wind speed for the day is used, which is 2 m/s. Inlet water temperature (T_in) is 30^{o} C. The ambient temperature reached 45^{o} C and irradiance, 860 W/m^2 (at 0^{o}). Maximum T_out of the water is 94^{o} C.

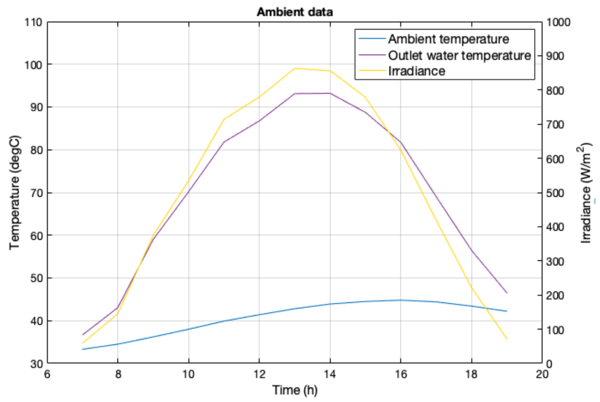

Figure 5.6: Weather data and maximum water outlet temperature, for a summer day in Dubai.

We find that T_ out curve depends on the irradiance and the ambient temperature. Similar curves for T_out with varying angle of tilt and flow rate were obtained. From these results, the average temperature difference between inlet and outlet water(ΔT) for the day, w.r.t tilt angle and flow rate was obtained in the contour plot seen in Figure 5.7(a). It is seen from the plot that ΔT is 44^{o} C for a flow rate of 9 l/h and inclination angle below 25^{o}, whereas it is 37^{o} C for a flow rate above 70 l/h and inclination angle of more than 20^{o}. Thus implying that ΔT is maximum for lower flow rates, and minimum for a higher flow rate, for this location in summer. This states that the T_out increases with a decrease in flow rate and vice versa. The tilt angle seems to makes a little difference on ΔT with these limited data points, in summer.

The red lines in the contour plots indicate current practical limits for the panel (Figure 5.7). The maximum inclination angle successfully tested was 8^{o}, above which the water in the reservoir leaked during experiments. Based on the value of maximum flow rate to the PV-T array in the plant design, the maximum flow rate through the panel is 25 l/h. Considering these, the bottom left quadrant (highlighted) is considered for optimum value selection. With optimisation in the panel design (to eliminate water leaks) and plant design (to increase the flow rate), these practical limits could change and the remaining sections of the plot could be used to obtain optimum values corresponding to those particular limits. Currently, the focus will be on this bottom left quadrant.

A plot showing the total efficiency of the PV-T panel through the day, as a function of tilt angle and flow rate is seen in Figure 5.7(b). It can be seen that the total efficiency is 66% for the angle of tilt below 12^{o} and flow rate

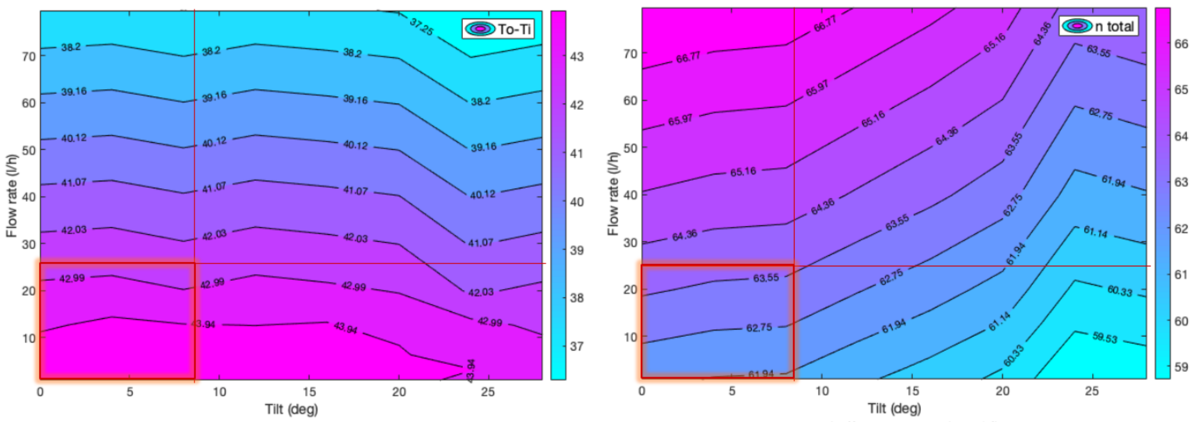

(a) Average temperature difference at the inlet and outlet.

(b) Total efficiency.

Figure 5.7: Average temperature difference and Total efficiency w.r.t tilt and flow rate for a summer day in Dubai.

of more than 70 l/h, whereas the total efficiency is 59% with a flow rate below 10l/h and angle of tilt above 22^{o}. Thus, **the total efficiency is higher for lower tilt angles and a higher flow rate while it decreases with a lower flow rate and higher tilt angle for the summertime**, for the used range of data.

Taking practical limits into account, the highlighted bottom left quadrant is taken into consideration for determining optimum values. From both the temperature difference and total efficiency plots, it is concluded that an inclination angle of 4^{o} and flow rate of 25 l/h is optimum, producing water at an average temperature of 72^{o} C (ΔT = 42^{o} C) and η_{total} = 63%.

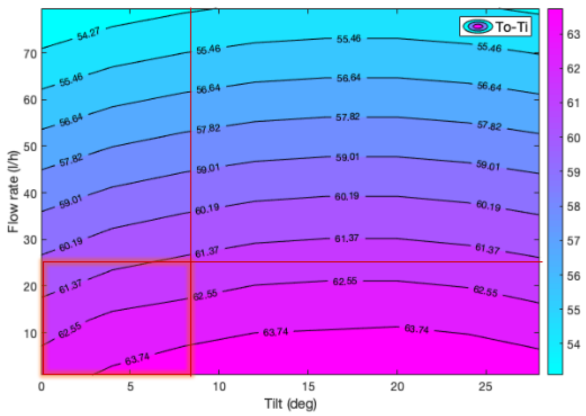

Figure 5.8: Maximum temperature difference at the inlet and outlet w.r.t tilt and flow rate for a summer day in Dubai.

Similar plots for the ΔT and η_{total} can be obtained for hourly values for a day. These are useful to determine optimum values in case a varying flow rate through the day is adapted for the plant design. The plot seen in Figure 5.8 reflects temperature difference during peak irradiance at 1 pm, w.r.t tilt and flow rate. It is seen that ΔT of 64^{o} C (T_out = 94^{o} C) can be achieved at a flow rate below 5 l/h and tilt angle between 4 to 8^{o}.

5.2.2. Winter day

The ambient data used for predicting the performance of the panel on a winter day and, the corresponding maximum outlet water temperature is shown in Figure 5.9. Average wind speed for the day was used, which is 2 m/s and T_in = 10^{o} C. The maximum ambient temperature is 18^{o} C and irradiance 620 W/m^{2} (at 0^{o}). Maximum T_out obtained is 58^{o} C.

Similar plots as seen earlier are made for ΔT and η_{total} as a function of tilt and flow rate. From the average ΔT plot (Figure 5.10(a)), it is seen that average ΔT is 34^{o} C for a flow rate below 10 l/h and angle of tilt above

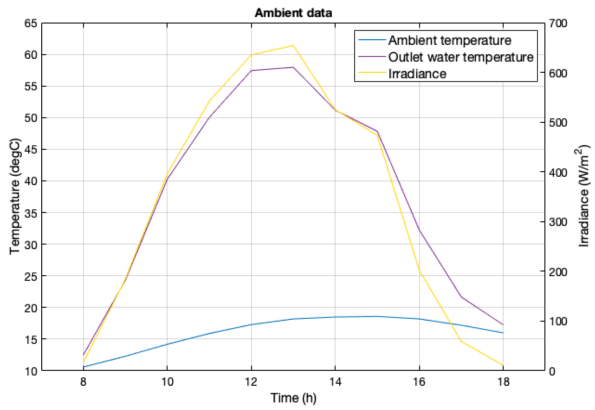

Figure 5.9: Weather data and maximum water outlet temperature, for a winter day in Dubai.

15^{o}, and 27^{o} C for a flow rate of 70 l/h and angle of tilt below 8^{o}. Thus, a higher temperature difference is achieved with a lower flow rate and higher tilt angle, whereas a lower temperature difference is obtained with a higher flow rate and lower tilt angle, in winter. The total efficiency as seen in Figure 5.10(b), increases with an increase in flow rate. η_{total} is 88% for a flow rate higher than 70 l/h and 77% for a flow rate lower than 10 l/h.

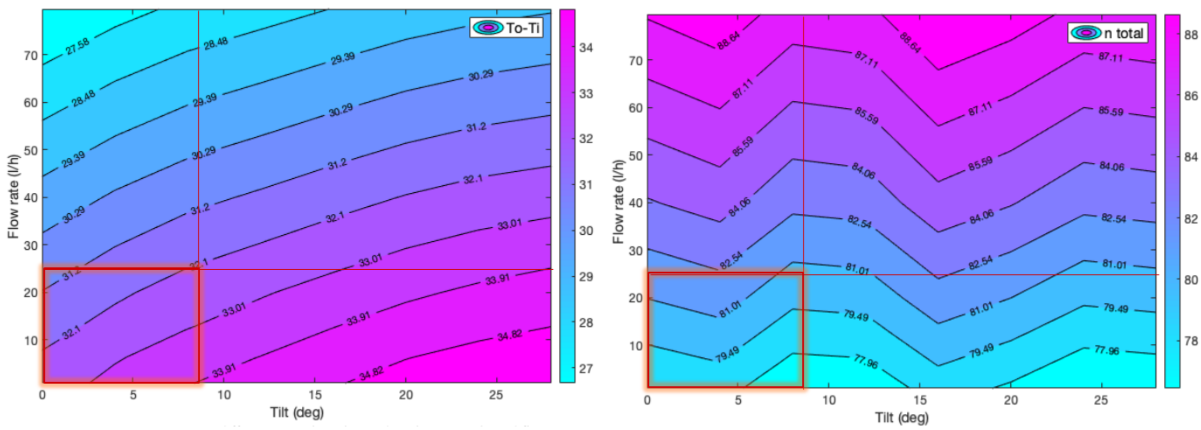

(a) Average temperature difference at the inlet and outlet.

(b) Total efficiency.

Figure 5.10: Average temperature difference and Total efficiency w.r.t tilt and flow rate for a winter day in Dubai.

Considering practical limits, the optimum tilt angle for winter is 8^{o} with a flow rate of 25 l/h. Hot water at T_out of 42^{o} C (ΔT = 32^{o} C) can be produced, with the maximum η_{total} of 79%.

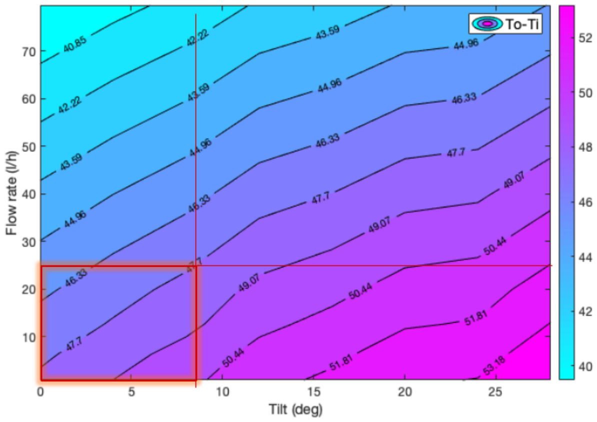

Figure 5.11: Maximum temperature difference at the inlet and outlet w.r.t tilt and flow rate for a winter day in Dubai.

Hourly T_out plot for the winter day suggests a maximum temperature of 59^o C (ΔT = 49^o C) can be achieved with the optimum tilt of 8^o and a flow rate below 5 l/h. (Figure 5.11)

5.3. Results for the location of West Bengal, India

Following the same procedure as for Dubai, results for the location of West Bengal for summer and winter days were obtained to study the change in optimum values based on this different weather data set. Inclination angles ranging from 0 to 16^o with a difference of 4^o were tested. For each of these tilt angles, results for flow rates ranging from 0 to 80 l/h were obtained.

5.3.1. Summer day

The ambient data for a summer day and the corresponding maximum outlet water temperature is seen in Figure 5.12. Average wind speed for the day is used, which is 1.5 m/s. Inlet water temperature is 30^o C. The maximum ambient temperature was 40^o C and irradiance (at 0^o) of 880 W/m^2. Maximum T_out from the panel is 92^o C.

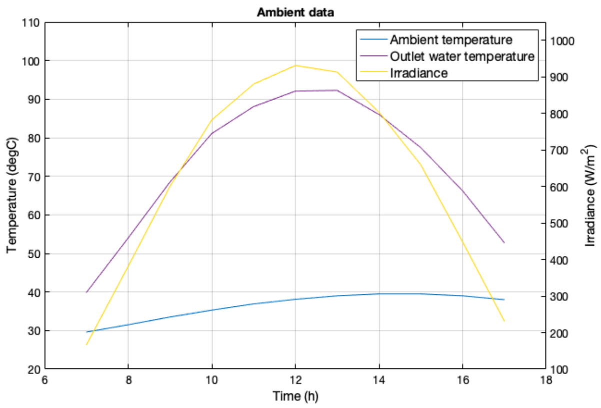

Figure 5.12: Weather data and maximum water outlet temperature, for a summer day in West Bengal.

Average ΔT and η_{total} as a function of tilt angle and flow rate is plot, along with the marked practical limits (Figure 5.13(a), 5.13(b)). The optimum tilt angle is 8^o C with a flow rate of 25 l/h, achieving a ΔT of 44^o C and η_{total} of 49%, in summer.

5.3.2. Winter day

The maximum ambient temperature for a winter day as seen in Figure 5.14 is 21^o C and the water outlet temperature 63^o C. The maximum value of irradiance is 670 W/m^2 (at 0^o). Average wind speed of 1.5 m/s is

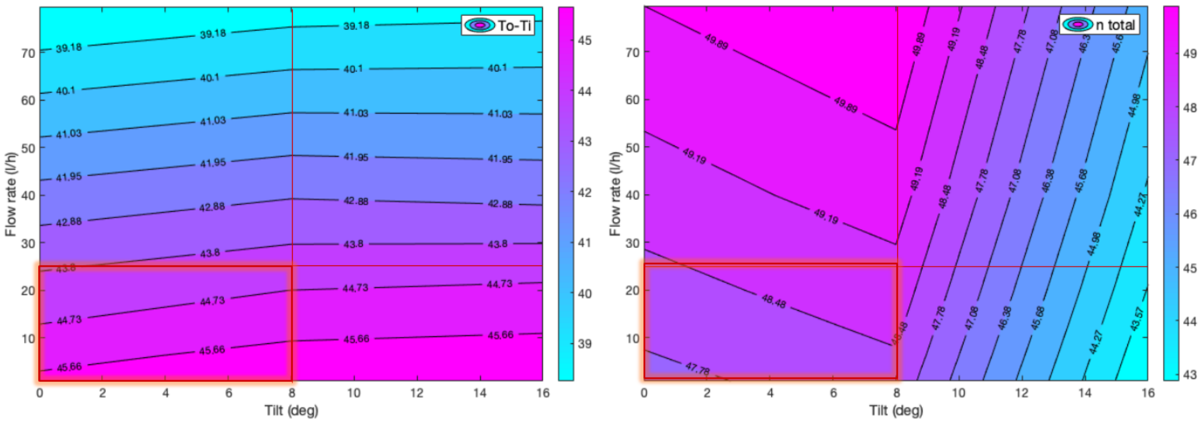

(a) Average temperature difference at the inlet and outlet.

(b) Total efficiency.

Figure 5.13: Average temperature difference and Total efficiency w.r.t tilt and flow rate for a summer day in West Bengal.

used and inlet water temperature of 10^{o} C. From contour plots for ΔT and η_{total} w.r.t tilt and flow rate (Figure 5.15(a), 5.15(b)), the optimum value of tilt and flow rate is obtained. An inclination angle of 8^{o} and a flow rate of 25 l/h yields a ΔT of 36^{o}C and η_{total} of 63%.

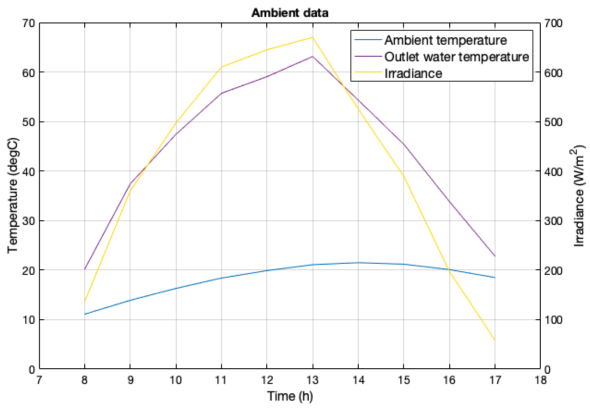

Figure 5.14: Weather data and maximum water outlet temperature, for a winter day in West Bengal.

5.4. Discussion

From the summer and winter results for both the locations of Dubai and West Bengal, it is seen that the **temperature difference between inlet and outlet increases when the flow rate decreases,** and temperature difference decreases when there is an increase in flow rate. This is in agreement with the works of Tiwari and Soda [48]. **The total efficiency, for both locations, increases with an increase in the flow rate.** A similar observation is recorded in previous works [34, 48]. A lower flow rate reduces the cooling effect of water on the cells, thus increasing temperatures and reducing the total efficiency. In summer, the water temperature difference between inlet and outlet is higher for a lower tilt angle (closer to 0^{o}), whereas for winter a higher tilt angle (towards 28^{o}) yields a greater temperature difference. As mentioned previously, the position of the sun changes based on the time and day of the year. During summer, the path of the sun is at a higher altitude compared to that in winter as seen in Figure 5.16. Due to the position of the sun, the irradiance on the PV module varies, which is a function of the angle of incidence on the module [46]. Therefore, for maximum incidence on the module, a higher tilt angle than summer is required during winter.

The outlet temperature and power output profile based on the optimum value of tilt angle and flow rate for both the locations is seen in Figure 5.17(a) and 5.17(b). The total efficiency is higher in winter than in summer (Figure 5.18(a) , 5.18(b)). This is due to higher ambient temperatures and thereby higher cell operating

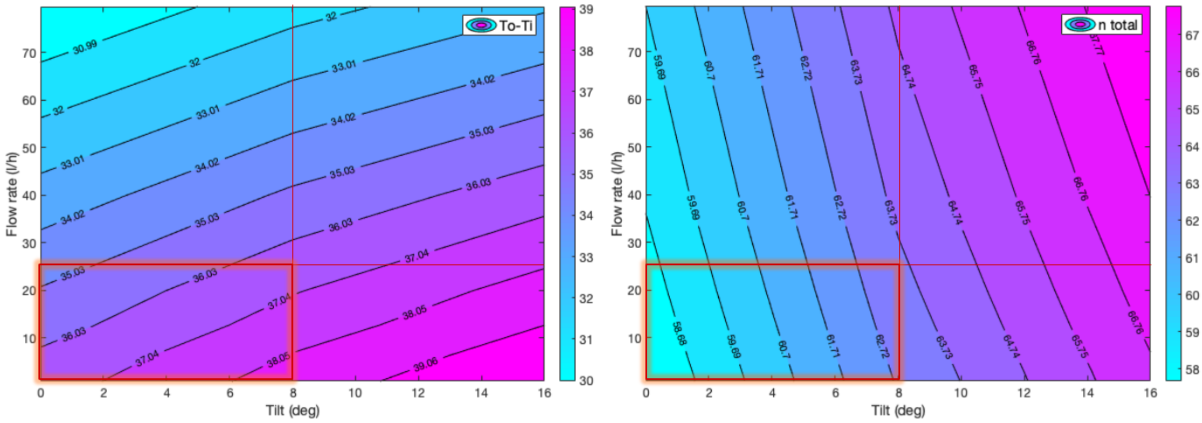

(a) Average temperature difference at the inlet and outlet.

(b) Total efficiency.

Figure 5.15: Average temperature difference and Total efficiency w.r.t tilt and flow rate for a winter day in West Bengal.

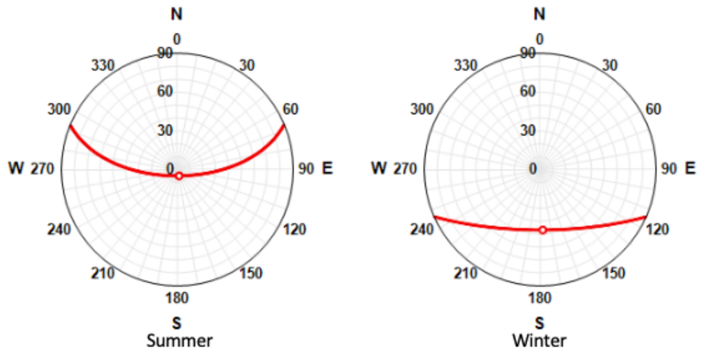

Figure 5.16: Sun path in Dubai for summer and winter.

temperatures in summer compared to winter. Higher cell temperatures result in degradation in the power output [40]. Table 5.1 shows a summary of the results for both locations for the different times of the year.

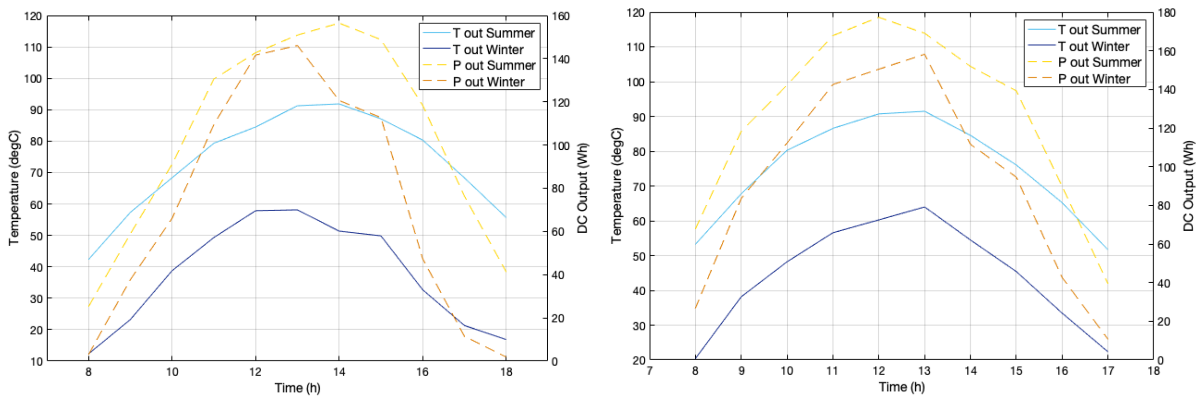

(a) Location: Dubai

(b) Location: West Bengal

Figure 5.17: Temperature and Power output for both the locations for optimum tilt and flow rate.

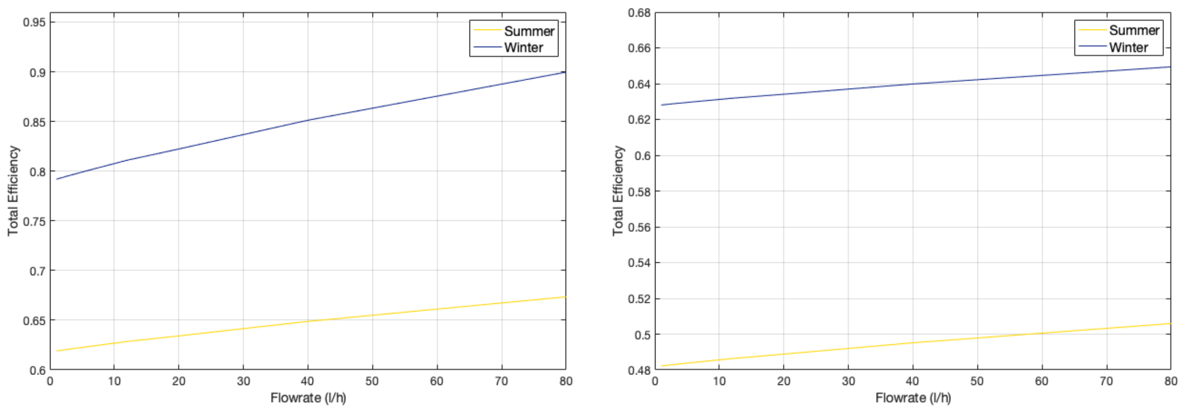

(a) Location: Dubai (b) Location: West Bengal

Figure 5.18: Total efficiency for summer and winter days w.r.t flow rate for for both the locations.

Table 5.1: Result summary.

Location	Dubai		West Bengal	
	Summer	Winter	Summer	Winter
Average T_out for the day(^{o} C)	72	42	74	46
Tilt angle (^{o})	4	8	8	8
Flow rate (l/h)	25	25	25	25
Total efficiency (%)	η_{th} = 52 ; η_{PV} = 11	η_{th} = 66 ; η_{PV} = 13	η_{th} = 37 ; η_{PV} = 12	η_{th} = 49 ; η_{PV} = 14
DC energy yield (kWh/day)	1.16	0.79	1.3	0.93

5.5. Buckingham's Pi theorem

As seen previously in Chapter 4 and in equation 5.2, an equation relating the temperature and physical quantities involved in the heat transfer through the panel was derived.

$$\Delta T = ql/k^* C(Re, Pr) \tag{5.2}$$

where ql/kΔT , v ρ l / μ and C_p μ / k are defined as the Nusselt, Reynolds and Prandtl numbers, respectively. As stated earlier, this equation shows that ΔT is a function of the solar irradiance, type of inlet fluid and its velocity, and the reservoir dimensions. The experimental and simulation results obtained for the inlet and outlet temperature difference are used in this equation to obtain the value of constant C. A linear relationship between these parameters is obtained as seen from Figure 5.19 and equation 5.3, for a range of Reynolds number (Re) from 19 to 1700.

$$\Delta T = ql/k^* \left(-3^* 10^{-4} Re + 3\right) \tag{5.3}$$

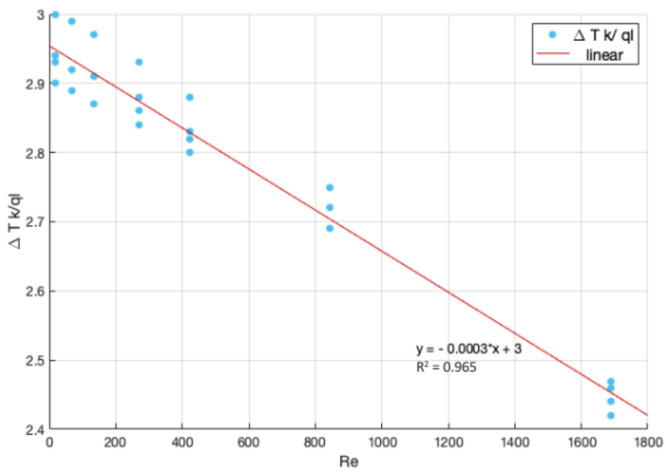

Figure 5.19: Relationship between Δ T k/ql vs Re.

Since the fluid in our case is water, Prandtl number (Pr) will always be always constant as it is a function of the fluid thermal properties. When a different fluid is used, Pr will vary according to the properties of heat capacity, thermal conductivity and dynamic viscosity of the chosen fluid.

Using this relationship from equation 5.3, an initial study for the maximum achievable temperature difference for a particular location can be done by using the irradiance (q), inlet velocity (v) and reservoir dimension parameters. It is especially useful for testing PV-T design parameters like type of fluid and the physical design of the panel, for example, the depth of the reservoir.

With properties of water (ρ , k , μ), current design (hydraulic diameter of reservoir = 0.0158 m) and operating conditions, for example, an irradiance of 860 W/m^2, and inlet velocity of 0.0008 m/s (0.9 l/h) Reynolds number = 19.19 is obtained. Using these in equation 5.3, ΔT of 64.8 K is obtained.

6

PV-T Panel to MED

The results obtained in the previous chapter for a single PV-T panel for the location of Dubai are scaled up to obtain results at the PV-T array level. The array consists of 400 PV-T panels. The output from the PV-T array is then used to calculate the amount of steam generated in the flash vessel which is used as input to the first effect of the MED. Finally, the output from the MED w.r.t steam generated in the flash vessel is obtained.

6.1. Flash evaporation

As seen from the results in the previous chapter, in table 5.1, the panel produces hot water at an average 72^o C on a summer day and hot water at an average 42^o C on a winter day. The maximum temperature of hot water that can be produced is 91^o C in summer and 58^o C in winter from the previous chapter (Figure 5.17(a)). The hot water produced from the panels is stored in insulated hot water tanks at atmospheric pressure.

The water stored in the hot water tanks is exposed to a lower pressure of 0.2 bar in the flash tank, thereby producing steam due to the latent heat of vaporisation. A study by Saury and Siroux states that the quantity of water flash evaporated is proportional to the superheat, which is defined as the temperature difference between the initial temperature of liquid water with its saturation temperature [43]. A higher initial temperature of liquid water produces a higher evaporated quantity of steam from flashing [29]. As discussed in section 3.4, the minimum temperature in the first MED effect must be 55^o C. Therefore, the flash vessel must provide steam at a minimum temperature of 60^o C. To obtain this, a higher average T_out from the panels must be obtained to be efficiently used for flashing.

The quantity of steam produced per kg of water is calculated by,

$$m_s = m_w \frac{c_p}{H_v}(T_{if} - T_{st}) \tag{6.1}$$

Where, m_s and m_w is the mass of steam and liquid water in kg, C_p is the specific heat capacity of water at initial temperature (J/kgK) H_v is the vaporisation enthalpy at saturation temperature (J/kg), and T_{if} and T_{st} is the initial and saturation temperature of water. (K)

Using this equation, the mass of steam produced per kg of water between 72^o C to 91^o C is calculated. (average and maximum temperature achievable in summer)

Table 6.1: Amount of steam produced per kg of water with different T_out from panel.

T_{if} (^{o}C)	Mass of steam (kg)/kg water
75	0.027
80	0.036
85	0.045
90	0.054

As seen in Table 6.1, a maximum of 0.054 kg of steam can be produced per kg water, at a temperature of 90^o C. However, a higher T_out yields a lower quantity of water from the panel, through the day, as from Figure 5.17(a), in the previous chapter, a T_out of 90^o C is obtained only for 2 hours between 1 pm to 3 pm, with a flow rate of 25 l/h. Therefore, further sensitivity analysis for the quantity of hot water produced w.r.t outlet temperature and corresponding steam produced for the PV-T array is done as seen in Table 6.2.

Table 6.2: Total amount of steam produced from water produced from the array.

T_{if} (^{o}C)	Mass of steam (kg)/kg water	Hot water (1 panel) (l/day)	Hot water (Array) (m^3)/day)	Mass of steam(kg)/day
75	0.027	>150	60	1600
80	0.036	>125	50	1780
85	0.045	>100	40	1782
90	0.054	>50	20	1070

It is seen that steam production from the flash vessel is maximum of 1782 kg for T_out of 85^o C from the PV-T array. Therefore, water from the PV-T panel at this average temperature should be obtained. This 1782 kg steam produced in the day is used as an input to the first MED effect.

As from Figure 5.17(a), in the previous chapter, it is seen that more than 100 l of water at T_out at 50^o C can be obtained during winter. Additional heating elements are required during these months to increase the temperature of water from 50 to 85^o C.

6.2. Output from PV-T Array

Using these values of T_out and the optimum value of flow rate (25 l/h) and tilt (4^o in summer, 8^o in winter) as defined in the previous chapter, a summary of output from a single panel and PV-T array is seen in Table 6.3 and for the array in Table 6.4, respectively.

Table 6.3: Output from a single PV-T panel.

Output from 1 PV-T panel	Summer (T_out=85^{o}C)	Winter (T_out =50^{o}C)
Hot water produced(l/day)	100	100

Table 6.4: Output from the PV-T Array.

Output from PV-T Array	Summer (T_out=85^{o}C)	Winter (T_out =50^{o}C)
Hot water produced(m^3/day)	40	40

6.3. Steam input to MED

The steam produced from the flash vessel is then used as an input to the first effect of MED, along with the steam produced by the MVC. The consumption of thermal energy in the process is given by the gained output ratio (GOR). It is defined as the ratio of the quantity of distilled water produced in kg, per kg of input steam. The GOR in a MED process depends on factors such as the number of effects, temperature and pressure of steam to the first effect, and feed water temperature [27]. From previously done mass balance calculations for the plant, a GOR of 3.4 was obtained.

$$GOR = \frac{\text{Mass of distillate produced (kg)}}{\text{kg of steam consumed}} \tag{6.2}$$

Using the GOR value in equation 6.2, the amount of distilled water produced per day, using steam produced in the flash vessel is calculated. 6058 kg of distilled water per day can be produced using steam from the flash vessel alone. Depending on the required quantity of distilled water, the MVC is required to provide the remaining steam input.

7 Conclusions and Recommendations

This chapter provides conclusions from the work carried out in this thesis and recommendations for future work.

A model of the Photovoltaic-Thermal (PV-T) panel has been developed using COMSOL Multiphysics and validated using experimental data to predict the design performance, in order to be used in the MED-MVC desalination plant of Desolenator. The use of this software allowed for the incorporation of the heat transfer mechanisms of conduction, convection, and heat loss mechanisms of convection instigated by wind as well as radiation from the panel surface to the surroundings.

Site-specific weather data of Dubai, for a summer and winter day, is used to obtain the electrical output predictions of the PV-T panels, using the PVMD Toolbox. The panel inclination angle range of 0 to 28^o and a Southwest orientation (reflecting the placement on-site) is used to obtain results, from which the electrical efficiency is calculated.

Absorption factors for layers within the module configuration are obtained using the GenPro4 tool. For the silicon layer, the efficiency value from Toolbox is subtracted from this so as to account for the portion of the heat lost due to conversion to electricity.

Weather data and these absorption values are used in the COMSOL model to obtain the hourly maximum achievable temperature of the outlet water from the panel. The summer maximum water outlet temperature is found to be 94^o C and the winter maximum water outlet temperature is 58^o C. From simulations, it is observed that the wind speed affects the water outlet temperature due to convection losses. The average water outlet temperature through the day for a wind speed of 1 m/s is found to be 88^o C whereas the average temperature is 80^o C for a wind speed of 2 m/s. Thus, higher wind speed results in lower water outlet temperatures due to higher convective heat loss and vice versa.

Simulations are performed for inclination angles ranging from 0 to 28^o and flow rates ranging from 0 to 80 l/h for a summer and winter day to obtain the hourly water outlet temperatures and to calculate the total efficiency (electrical + thermal) of the PV-T module. Using these results, an optimum tilt angle and flow rate for summer and winter months are obtained while taking practical limits into account (tilt at which there are no water leaks and the maximum flow rate through the panel). For summer, the optimum tilt is 4^o and for winter is 8^o. The optimum flow rate for both summer and winter months is 25 l/h. It is found that a higher flow rate yields lower water outlet temperatures whereas a lower flow rate yields higher water outlet temperatures. The total efficiency, however, increases with an increasing flow rate, for the simulated range. A ΔT of 44^o C is obtained with a flow rate below 10 l/h whereas ΔT of 37^o C is obtained with a flow rate of 70 l/h, in summer. While in winter, ΔT of 34^o C is obtained with a flow rate below 10 l/h and ΔT of 27^o C is obtained with a flow rate of 70 l/h.

The average temperature of water produced in the day and the total efficiency, using these optimum values of tilt and flow rate is 72^o C and 63% (11% η_{PV}) respectively, in summer, vs 42^o C and 79% (13% η_{PV}) respectively, in winter. It is found that the total efficiency is higher in winter compared to summer. This is due to higher ambient temperatures in summer leading to higher operating cell temperature compared to winter months.

The DC yield from a single panel using the optimum values for summer and winter is 1.16 kWh/day and 0.79 kWh/day, respectively.

A similar sensitivity study for a different location of West Bengal with south-facing panels was performed. Results suggest an optimum angle and flow rate of 8^o and 25 l/h respectively for summer and winter, with average water outlet temperature of 74 ^{o} C and 46^o C for summer and winter days, respectively. The DC yield obtained is 1.3 kWh/day in summer and 0.93 kWh/day in winter.

A relationship is derived between the water temperature difference between the inlet and outlet and the Nusselt, Reynolds and Prandtl numbers using the data from experimental and simulated values. The Nusselt, Reynolds and Prandtl numbers are ratios of the properties of fluid, inlet flow, and the module geometry. The relationship states that ΔT is a function of the solar irradiance, type of inlet fluid and its velocity, and the reservoir dimensions- $\Delta T = ql/k^* \left(-3^* 10^{-4} Re + 3\right)$
where, ql/kΔT , v ρ l / μ and C_p μ / k are defined as the Nusselt, Reynolds and Prandtl numbers respectively. If these parameters are known, the maximum achievable water temperature difference between inlet and outlet can be obtained. This can be used as an initial feasibility study for the location, type of the fluid or even the reservoir dimensions.

The hot water produced from the PV-T array (400 PV-T panels) is used in the flash vessel to produce steam to be used as an input to the first effect of the MED vessel. With a sensitivity analysis for the amount of hot water that can be produced w.r.t water outlet temperatures, the maximum quantity of steam production in the flash vessel, in a summer day is obtained. It is found that the maximum steam production of 1782 kg is obtained with a water outlet temperature of 85^o C. Finally, using the gain output ratio of 3.4 for the MED, it is found that 6058 kg of distilled water is produced using this steam produced in the flash vessel. Depending on the requirement of water production, the remaining steam input can be supplied by the MVC.

Further work can be carried out on the COMSOL model, PV-T design, and plant design. Since the model is computationally expensive, studies into reducing this computational strain should be undertaken. The PV-T module design performance can be studied without the top glass cover. It is found from literature that losses in electrical efficiency can be reduced by up to 0.8% by removing the top glass cover. However, an uncovered system reduces the thermal efficiency of the system [55]. Depending on the performance of the system under this scenario, its use in applications requiring a low-temperature outlet can be investigated, for example, hot water for domestic use. A higher absorption factor of the solar cell corresponds to a higher thermal efficiency of the module. With a 20% increase in the absorption factor, an 8% increase in the thermal efficiency was observed [39]. A study of suitable thin-film PV technologies with a higher absorption factor than the current design, to be used in the PV-T module can be undertaken. Also, cell technology with a lower power temperature coefficient can be investigated to reduce the loss in output due to higher cell operating temperatures. Variations to the reservoir design, for example, varying the reservoir depth, or by adding sections within the reservoir can be studied. For the plant study, analysis of the total energy production and requirement with storage should be performed.

Bibliography

[1] 2030 WRG (2030 Water Resources Group). Charting our Water Future: Economic Frameworks to Inform Decision-making., 2009. Available at https://www.mckinsey.com/~/media/mckinsey/dotcom/client_service/sustainability/pdfs/charting%20our%20water%20future/charting_our_water_future_full_report_.ashx, Last retrieved on 07-08-2020.

[2] A.L Abdullah, Suhaimi Misha, N Tamaldin, M.A. Mohd Rosli, and F.A Sachit. Technology progress on photovoltaic thermal (pvt) systems with flat-plate water collector designs: A review. *Journal of Advanced Research in Fluid Mechanics and Thermal Sciences*, 59:107–141, 2019.

[3] Ali Al-Karaghouli and Lawrence L Kazmerski. Energy consumption and water production cost of conventional and renewable-energy-powered desalination processes. *Renewable and Sustainable Energy Reviews*, 24:343–356, 2013.

[4] V Belessiotis and E Delyannis. Water shortage and renewable energies (re) desalination—possible technological applications. *Desalination*, 139(1-3):133–138, 2001.

[5] Theodore L Bergman, Adrienne Lavine, Frank P Incropera, and David P Dewitt. *Fundamentals of heat and mass transfer*. John Wiley & Sons New York, 2017.

[6] Jiajun Cen, Roan du Feu, Matus E Diveky, Catriona McGill, Oliver Andraos, and William Janssen. Experimental study on a direct water heating pv-t technology. *Solar Energy*, 176:604–614, 2018.

[7] PG Charalambous, Graeme G Maidment, Soteris A Kalogirou, and K Yiakoumetti. Photovoltaic thermal (pv/t) collectors: A review. *Applied thermal engineering*, 27(2-3):275–286, 2007.

[8] COMSOL. Heat Transfer Module. User's Guide v 5.4., . Available at https://doc.comsol.com/5.4/doc/com.comsol.help.heat/HeatTransferModuleUsersGuide.pdf., Last retrieved on 07-08-2020.

[9] COMSOL. Building the Mesh for a Model Geometry in COMSOL Multiphysics., . Available at https://www.comsol.nl/video/building-the-mesh-for-a-model-geometry-in-comsol-multiphysics., Last retrieved on 07-08-2020.

[10] COMSOL. The Finite Element Method (FEM)., 2016. Available at https://www.comsol.nl/multiphysics/finite-element-method., Last retrieved on 07-08-2020.

[11] PK Dash and NC Gupta. Effect of temperature on power output from different commercially available photovoltaic modules. *International Journal of Engineering Research and Applications*, 5(1):148–151, 2015.

[12] Alberto de la Calle, Javier Bonilla, Lidia Roca, and Patricia Palenzuela. Dynamic modeling and simulation of a solar-assisted multi-effect distillation plant. *Desalination*, 357:65–76, 2015.

[13] E-E Delyannis. Status of solar assisted desalination: a review. *Desalination*, 67:3–19, 1987.

[14] T Dembeck-Kerekes, Jamie P Fine, J Friedman, SB Dworkin, and JJ McArthur. Performance of variable flow rates for photovoltaic-thermal collectors and the determination of optimal flow rates. *Solar Energy*, 182:148–160, 2019.

[15] Desolenator. MED-MVC desalination plant components, 2020. Retrieved from internal communication with Jiajun Cen.

[16] Mohamed L Elsayed, Osama Mesalhy, Ramy H Mohammed, and Louis C Chow. Transient and thermo-economic analysis of med-mvc desalination system. *Energy*, 167:283–296, 2019.

[17] Engineering ToolBox. Emissivity Coefficients Materials., 2003. Available at `https://www.engineeringtoolbox.com/emissivity-coefficients-d_447.html.`, Last retrieved on 07-08-2020.

[18] C Frantz and B Seifert. Thermal analysis of a multi effect distillation plant powered by a solar tower plant. *Energy Procedia*, 69:1928–1937, 2015.

[19] Elias Garcia Goma. Development of cell to system annual energy yield toolbox for bifacial modules. 2018.

[20] Lourdes Garcia-Rodriguez, Ana I Palmero-Marrero, and Carlos Gómez-Camacho. Comparison of solar thermal technologies for applications in seawater desalination. *Desalination*, 142(2):135–142, 2002.

[21] Julen Garro Etxebarria. Toolbox for the design and simulation of a floating bifacial pv plant with reflectors. 2018.

[22] HMS Hussein, GE Ahmad, and HH El-Ghetany. Performance evaluation of photovoltaic modules at different tilt angles and orientations. *Energy conversion and management*, 45(15-16):2441–2452, 2004.

[23] JK Kaldellis, D Zafirakis, EL Kaldelli, and K Kavadias. Cost benefit analysis of a photovoltaic-energy storage electrification solution for remote islands. *Renewable energy*, 34(5):1299–1311, 2009.

[24] Soteris Kalogirou. Survey of solar desalination systems and system selection. *energy*, 22(1):69–81, 1997.

[25] Soteris A Kalogirou. Use of trnsys for modelling and simulation of a hybrid pv–thermal solar system for cyprus. *Renewable energy*, 23(2):247–260, 2001.

[26] Soteris A Kalogirou. Seawater desalination using renewable energy sources. *Progress in energy and combustion science*, 31(3):242–281, 2005.

[27] RK Kamali, A Abbassi, SA Sadough Vanini, and M Saffar Avval. Thermodynamic design and parametric study of med-tvc. *Desalination*, 222(1-3):596–604, 2008.

[28] Kate Fried, Food and Water Watch. Ocean Desalination No Solution to Water Shortages., 2009. Available at `https://www.foodandwaterwatch.org/news/ocean-desalination-no-solution-water-shortages`, Last retrieved on 07-08-2020.

[29] W Kays, ME Crawford, and B Weigand. Turbulent prandtl number. *Convective heat and mass transfer, Fourth edition ed: McGRAW-HILL*, pages 233–239, 2005.

[30] Huanmin Lu, John C Walton, and Andrew HP Swift. Desalination coupled with salinity-gradient solar ponds. *Desalination*, 136(1-3):13–23, 2001.

[31] Akbar Maleki and Alireza Askarzadeh. Optimal sizing of a pv/wind/diesel system with battery storage for electrification to an off-grid remote region: A case study of rafsanjan, iran. *Sustainable Energy Technologies and Assessments*, 7:147–153, 2014.

[32] Agustín Aragón Mesa, Claudio Miguez Gómez, and Ramón Urcelay Azpitarte. Energy saving and desalination of water. *Desalination*, 108(1-3):43–50, 1997.

[33] Meteornom. Global Meteorological Database. Available at `https://meteonorm.com/.`, Last retrieved on 07-08-2020.

[34] Jai Prakash. Transient analysis of a photovoltaic-thermal solar collector for co-generation of electricity and hot air/water. *Energy Conversion and Management*, 35(11):967–972, 1994.

[35] Hazim Mohameed Qiblawey and Fawzi Banat. Solar thermal desalination technologies. *Desalination*, 220(1-3):633–644, 2008.

[36] React Europe. Thermal insulation materials: Polyurethane (PUR) and Polyisocyanurate (PIR) foam. Available at `https://pdf4pro.com/view/thermal-insulation-materials-polyurethane-pur-1ba65.html.`, Last retrieved on 07-08-2020.

[37] G Maheedhara Reddy and V Diwakar Reddy. Theoretical investigations on dimensional analysis of ball bearing parameters by using buckingham pi-theorem. *Procedia Engineering*, 97:1305–1311, 2014.

[38] BjØrnar Sandnes and John Rekstad. A photovoltaic/thermal (pv/t) collector with a polymer absorber plate. experimental study and analytical model. *Solar Energy*, 72(1):63–73, 2002.

[39] R Santbergen, VA Muthukumar, RME Valckenborg, WJA van de Wall, AHM Smets, and M Zeman. Calculation of irradiance distribution on pv modules by combining sky and sensitivity maps. *Solar Energy*, 150:49–54, 2017.

[40] Rudi Santbergen. Optical absorption factor of solar cells for pvt systems. *Technische Universiteit Eindhoven*, 2008.

[41] Rudi Santbergen, Tomomi Meguro, Takashi Suezaki, Gensuke Koizumi, Kenji Yamamoto, and Miro Zeman. Genpro4 optical model for solar cell simulation and its application to multijunction solar cells. *IEEE journal of photovoltaics*, 7(3):919–926, 2017.

[42] Junainah Sardi, Nadarajah Mithulananthan, Marcus Gallagher, and Duong Quoc Hung. Multiple community energy storage planning in distribution networks using a cost-benefit analysis. *Applied energy*, 190:453–463, 2017.

[43] Didier Saury, S Harmand, and M Siroux. Experimental study of flash evaporation of a water film. *International Journal of Heat and Mass Transfer*, 45(16):3447–3457, 2002.

[44] Patricia Seoane da Silva. Infrared optical filters for passive cooling of crystalline silicon modules. 2017.

[45] MA Sharaf, AS Nafey, and Lourdes García-Rodríguez. Thermo-economic analysis of solar thermal power cycles assisted med-vc (multi effect distillation-vapor compression) desalination processes. *Energy*, 36 (5):2753–2764, 2011.

[46] Arno Smets, Klaus Jäger, Olindo Isabella, René Van Swaaij, and Miro Zeman. The physics and engineering of photovoltaic conversion, technologies and systems. *Solar Energy. Cambridge: UIT*, 2015.

[47] Alon Tal. Addressing desalination's carbon footprint: the israeli experience. *Water*, 10(2):197, 2018.

[48] Arvind Tiwari and MS Sodha. Performance evaluation of hybrid pv/thermal water/air heating system: a parametric study. *Renewable energy*, 31(15):2460–2474, 2006.

[49] Ihsan Ullah and Mohammad G Rasul. Recent developments in solar thermal desalination technologies: A review. *Energies*, 12(1):119, 2019.

[50] UN Water. The UN World Water Development Report 2020: Water and Climate change., 2020. Available at `https://unesdoc.unesco.org/ark:/48223/pf0000372985.locale=en`, Last retrieved on 07-08-2020.

[51] Bart Van der Bruggen and Carlo Vandecasteele. Distillation vs. membrane filtration: overview of process evolutions in seawater desalination. *Desalination*, 143(3):207–218, 2002.

[52] Silvano Vergura, Giuseppe Acciani, and Ottavio Falcone. A finite-element approach to analyze the thermal effect of defects on silicon-based pv cells. *IEEE Transactions on Industrial Electronics*, 59(10):3860–3867, 2011.

[53] World Water Council. Water Futures., 2019. Available at `https://www.worldwatercouncil.org/fileadmin/wwc/Library/WWVision/Chapter3.pdf`, Last retrieved on 07-08-2020.

[54] Leonid P Yarin. *The Pi-Theorem: applications to fluid mechanics and heat and mass transfer*, volume 1. Springer Science & Business Media, 2012.

[55] HA Zondag, DW De Vries, WGJ Van Helden, RJC Van Zolingen, and AA Van Steenhoven. The yield of different combined pv-thermal collector designs. *Solar energy*, 74(3):253–269, 2003.

[56] Herman A Zondag, DW de de Vries, WGJ Van Helden, RJ Ch van Zolingen, and AA Van Steenhoven. The thermal and electrical yield of a pv-thermal collector. *Solar energy*, 72(2):113–128, 2002.